Impaired bidirectional communication between interneurons and oligodendrocyte precursor cells affects cognitive behavior

Lipao Fang[1], Na Zhao[1], Laura C. Caudal[1], Renping Zhao[2], Ching-Hsin Lin[3], Hsin-Fang Chang[3], Nadine Hainz[4], Carola Meier[4], Bernhard Bettler[5], Wenhui Huang[1], Anja Scheller[1], Frank Kirchhoff[1,*], Xianshu Bai[1,*]

1. Molecular Physiology, CIPMM, University of Saarland, 66421 Homburg, Germany
2. Biophysics, CIPMM, University of Saarland, 66421 Homburg, Germany
3. Cellular Physiology, CIPMM, University of Saarland, 66421 Homburg, Germany
4. Department of Anatomy and Cell Biology, University of Saarland, 66421 Homburg, Germany
5. Department of Biomedicine, University of Basel, 4056 Basel, Switzerland

Correspondence to:

Prof. Dr. Frank Kirchhoff,
Molecular Physiology,
CIPMM, University of Saarland,
66421 Homburg, Germany
frank.kirchhoff@uks.eu

Dr. Xianshu Bai
Molecular Physiology,
CIPMM, University of Saarland,
66421 Homburg, Germany
xianshu.bai@uks.eu

Abstract

Cortical neural circuits are complex but very precise networks of balanced excitation and inhibition (E/I). Yet, the molecular and cellular mechanisms that form the E/I balance are just beginning to emerge. Here, using conditional $GABA_B$ receptor-deficient mice we identified a GABA/TNF-related cytokine (TNFSF12)-mediated bidirectional communication pathway between Parvalbumin-positive (PV^+) fast spiking interneurons and oligodendrocyte precursor cells (OPCs) that determines the density and function of interneurons in the developing medial prefrontal cortex (mPFC). Interruption of the GABAergic signaling to OPCs resulted in reduced myelination and hypoactivity of interneurons, strong changes of cortical network activities and impaired cognitive behavior. In conclusion, glial transmitter receptors are pivotal elements in finetuning distinct brain functions.

Introduction

The inhibition of cortical network activity is performed by interneurons that release the inhibitory transmitter γ-aminobutyric acid (GABA) which acts on ionotropic $GABA_A$ and metabotropic $GABA_B$ receptors ($GABA_BR$) [1, 2]. Alterations of interneuron cell density as well as concomitant changes of firing activity are often observed in several neuropsychiatric conditions [3-6]. In the mouse cortex, higher frequencies of spontaneous inhibitory postsynaptic currents (sIPSCs) were observed after increasing the interneuron density by transplantation of precursor cells [7]. Similarly, blocking of interneuron apoptosis caused a decrease of the excitation/inhibition (E/I) ratio [6, 8]. Interneuron density is a pivotal determinant of correct inhibitory circuits in the central nervous system (CNS). During development, a surplus of interneurons is generated that populates the cortical plate [9]. Subsequently, about 40 % of cortical inhibitory neurons are eliminated by programmed cell death during the first two postnatal weeks

52 [7]. One hypothesis links the apoptosis of supernumerary neurons with the onset of first
53 neuron-neuron connections [10]. Only the neurons that receive sufficient neurotrophic
54 signals from their target cells will survive [10, 11].

55 Oligodendrocyte precursor cells (OPCs) form synapses with interneurons as early as
56 postnatal day (p) 4-5 [12]. Concomitantly, the incidence of interneuron apoptosis
57 increases drastically after p5 and reaches its peak at p7 [7]. Right after, the interneuron-
58 OPC connectivity accelerates till p10, which drives an immediate oligodendrocyte (OL)
59 boom and subsequent interneuron myelination via OPC-$GABA_A$ and $GABA_B$ receptors
60 [13-15]. Despite relatively short axons, myelination of cortical interneurons (mainly
61 parvalbumin $(PV)^+$ fast-spiking interneurons, [16]) contributes significantly to the fine-
62 tuning of local activity in the medial prefrontal cortex (mPFC) and cortex, ensuring
63 proper performance of behavior [4, 17]. However, how the early communication between
64 interneuron and OPC affect inhibitory network activity in the mPFC still remains
65 unknown.

66 To assess the function of OPC $GABA_B$Rs for mPFC inhibition, we conditionally deleted
67 the $GABA_B$ receptor subunit *gabbr1* selectively in OPCs at the end of the first postnatal
68 week. By focusing on the medial prefrontal cortex (mPFC), we found that OPCs shape
69 the inhibitory network by $GABA_B$ receptor and the cytokine tumor necrosis factor-like
70 weak inducer of apoptosis (TWEAK) signaling pathways, thereby finetuning
71 interneuron cell death and survival as well as its myelination onset. The functional and
72 morphological changes of PV^+ interneurons observed in the adult mPFC of mutant
73 mice generate a reduction of the inhibitory tone, which finally leads to impaired
74 cognition and social behavior.

75

76 **Results**

77 *$GABA_B$Rs of OPCs are required for oligodendrogenesis in the mPFC*

78 To assess the function of $GABA_B$Rs for OPC-interneuron communication, we
79 generated Tg*(NG2-CreER^{T2}):$GABA_{B1}R^{fl/fl}$* mice (Fig. 1a) to conditionally knockout
80 (cKO) functional $GABA_B$R from OPCs and their progeny. We induced the cKO at
81 postnatal day 7 and 8 (p7/8) before the onset oligodendrocyte formation at p10-11 [13].
82 When analyzed at the age of 9 weeks (w), about 80 % of OPCs (platelet-derived
83 growth factor receptor α^+ (PDGFRα^+, Pα+))were found recombined (Pα^+tdT$^+$/Pα^+) in
84 the medial prefrontal cortex (mPFC), based on tdTomato (tdT) gene expression
85 (Fig. 1b, c).

86 To confirm and quantify the deletion of $GABA_B$R in OPCs, we performed Western blot
87 analysis with OPCs purified by magnetic-activated cell sorting (MACs-OPCs). In cKO
88 OPCs, $GABA_B$R expression was reduced by about 64 % compared with controls (ctl)
89 (Fig. 1d). Considering the substantial purity of MACS-sorted OPCs (85 %, data not
90 shown) and recombination efficiency (80 %), we concluded that a vast majority of
91 $GABA_B$Rs had been ablated from OPCs.

92 Next, we focused on the oligodendrocyte lineage and evaluated the contribution of
93 $GABA_B$Rs for OPC differentiation in the mPFC by immunostaining of PDGFRα and
94 adenomatous polyposis coli clone 1 (CC1) (Fig. 1e), established markers for OPCs
95 and oligodendrocytes, respectively. In the cKO mice, the density of OPCs
96 (PDGFRα^+Olig2$^+$) did not change (Fig. 1f), while that of mature oligodendrocytes
97 (CC1$^+$Olig2$^+$) was strongly reduced to 74 % (Fig. 1g), indicative of decreased OPC
98 differentiation to oligodendrocytes (Fig. 1h). Notably, in the corpus callosum the
99 densities of oligodendrocytes and OPCs, as well as their relative proportions did not
100 differ between ctl and cKO mice (Fig.1 f-h, Extended Data Fig. 1). These data suggest

101 that OPC-$GABA_B$Rs are required for OPC differentiation in the grey matter mPFC, but
102 not in the white matter corpus callosum.

103 We further analyzed structural aspects of myelination which is important for axonal
104 conductivity, i.e. the lengths of nodes (the gaps between paired contactin-associated
105 protein-positive ($Caspr^+$) segments) and paranodes (single $Caspr^+$ segments) by
106 immunostaining (Fig. 1i). In cKO mPFC, the paranodal length was increased (Fig. 1j)
107 while node length and density remained stable (Extended Data Fig. 2). In parallel, we
108 observed a reduction of myelin basic protein (MBP) expression at the mRNA
109 (Extended Data Fig. 2) and protein levels (Fig. 1k) in cKO mPFC, while the other
110 myelin protein, proteolipid protein (PLP) mRNA levels were not changed (Extended
111 Data Fig. 2). In the corpus callosum, however, myelination was unperturbed as
112 indicated by unchanged paranode length (Extended Data Fig. 2), node density
113 (Extended Data Fig. 2) and MBP expression (Fig. 1k). Therefore, our data show that
114 $GABA_B$Rs of OPCs promote differentiation and myelination in the mPFC, but do not
115 affect the corpus callosum.

116 Since OPCs continuously differentiate into oligodendrocytes [18-20], the cKO mice will
117 also generate oligodendrocytes lacking $GABA_B$Rs. To selectively target only
118 oligodendrocytes, we used Tg*(PLP-Cre^{ERT2}):GABA$_{B1}$R$^{fl/fl}$* mice (Extended Data Fig. 3) .
119 The gene deletion was induced by tamoxifen injections at p7/8 or at 4w. At the age of
120 9w, we did not observe differences in the OPC and oligodendrocyte population
121 between ctl and cKO mice (Extended Data Fig. 3), neither in the PFC nor in the corpus
122 callosum (Extended Data Fig. 3).

123 In summary, our data strongly suggest that $GABA_B$R is specifically required for early
124 OPC differentiation and subsequent myelination in the mPFC, but not in the corpus
125 callosum.

126

127 *$GABA_BRs$ of OPCs promote the myelination of interneurons in the mPFC*

128 Since callosal axons are primarily excitatory [21] and axons of inhibitory interneurons are
129 largely restricted to cortical areas of the same hemisphere (including mPFC, Fig.1l)
130 (Extended Data Fig. 4), we hypothesized that the observed myelin deficits were
131 restricted to interneurons. Required by their fast-spiking activity, parvalbumin $(PV)^+$
132 interneurons are the most abundantly myelinated interneurons [16, 22-24] of the cortex.
133 These neurons are most prominent at the layer 4 and 5 with majority of their axons
134 projecting to the layer 2/3 and 5 [25] (Fig. 1l, Extended Data Fig. 4). To evaluate their
135 myelination, we performed PV and MBP double immunostaining (Fig. 1l-n) and
136 analyzed the volume of myelin sheaths, by volume rendering of MBP immunolabel
137 covering PV^+ axons at the cortical layers 2/3 of mPFC. Indeed, the volume of myelin
138 sheaths wrapping PV neurons was reduced by 60 % in the cKO mPFC (Fig. 1n).
139 However, the myelination of excitatory neurons (in the corpus callosum) was not
140 affected as the g-ratio of myelinated axons and conduction velocity of compound action
141 potential did not differ between ctl and cKO mice (Extended Data Fig. 2). Thus, we
142 concluded that $GABA_BR$ of OPCs are preferentially involved in the myelination of
143 inhibitory rather than excitatory neurons.

144

145 *Postnatal deletion of $GABA_BRs$ in OPCs causes enhanced interneuron density in the*
146 *adult, but with reduced GABA release*

147 While investigating the interneuronal myelination, we recognized that early ablation of
148 $GABA_BR$ in OPCs (at p7/8, Fig. 2a) was associated with a 30 % increase of interneuron
149 density (10.4 vs 13.3 for ctl and cKO respectively) in the cortex as revealed by
150 immunostaining for PV (Fig. 2b). However, in the mPFC this increase did not result in
151 a concomitant increase of inhibitory input (Fig. 2c, d). In contrast, the frequency of
152 spontaneous inhibitory postsynaptic currents (sIPSCs) of pyramidal neurons in the

153 layer V of mPFC, where interneurons are abundantly located, was reduced by 40 %,
154 while the amplitude of sIPSCs remained unaffected in the mutant mPFC as well as the
155 firing rate and amplitude of excitatory postsynaptic currents (EPSCs).

156 Since neuronal activity can regulate myelination [22, 26], we asked whether the reduced
157 inhibitory firing rate contributed to the observed molecular and structural changes of
158 the myelin at interneuronal axons in the mutant mPFC. For that purpose, we further
159 analyzed the cKO mPFC of p10 mice (Fig. 2e) at the onset of myelination and when
160 interneuron-OPC communication peaks [13]. After induction of the cKO at p7/8, we
161 assessed the density of the vesicular GABA transporter (vGAT) close to OPC surfaces
162 as a quantitative readout of inhibitory presynaptic terminals by combined vGAT and
163 PDGFRα immunostaining [27] (Fig. 2f-i, Extended Data Fig. 5). We classified the vGAT
164 puncta into two subgroups based on the distance between vGAT staining and OPC
165 surface: '<20 nm' as vesicles targeting on postsynaptic OPCs (magenta), and '>20 nm'
166 as vesicles targeting on other cells (grey), assuming a width of about 20 nm for the
167 synaptic cleft [28]. And indeed, already at p10, i.e. only 3 days after the first tamoxifen
168 injection, the density and the volume of vGAT immunopuncta were reduced were
169 reduced to 75 % and 80 % in the cKO mPFC (Fig. 2f-i, Extended Data Fig. 5), including
170 a smaller volume of vGAT (Fig. 2h) and less puncta (Fig. 2i) at the OPC surface in
171 cKO mPFC, which can explain the attenuated firing rate of the interneurons in the adult.
172 These results indicate that interneurons exhibit lower activity and transmit less
173 GABAergic signals to OPCs in the cKO mPFC.

174 To test whether the reduced inhibitory tone affecting OPC differentiation specifically
175 correlates with the onset of myelination, we compared the OPC and oligodendrocyte
176 populations at p10 and p14 (Fig. 2j-m, Extended Data Fig. 6). At p10, the densities of
177 OPC and oligodendrocyte populations were still comparable in the cKO mPFC to
178 control mPFC, although the interneurons already expressed less vGAT (Fig. 2f-h).
179 However, at p14, the differentiation and cell numbers of oligodendrocytes dropped

180 strongly in the mutant mPFC (Fig. 2l, Extended Data Fig. 6), as did the MBP
181 expression (Fig. 2m). Again, in the corpus callosum, OPC and oligodendrocyte
182 population were not affected by the deletion of $GABA_BRs$ (Extended Data Fig. 1).

183 When we induced $GABA_BR$ deletion in the young adult mice at the age of 4 weeks,
184 both in the mPFC and corpus callosum, the density of oligodendrocyte as well as the
185 MBP expression were not affected in the cKO mice (Extended Data Fig. 7).

186 In summary, our data strongly suggest that during early development of the mPFC
187 deletion of $GABA_BR$ in OPCs affects the inhibitory tone of interneurons, feeding back
188 onto OPC differentiation and interneuron myelination.

189

190 *OPCs induce interneuron apoptosis via $GABA_BR$-TWEAK signaling*

191 As we had seen a surplus of interneurons in the mutant mPFC which could explain the
192 abnormal neuronal activity [8, 29], we tested whether the interneuron numbers would be
193 accurately controlled by programmed cell death early during development. After
194 induction of $GABA_BR$ in OPCs at p7/8, the extent of interneuron apoptosis was
195 determined at p10 and p14 by immunostaining for PV and cleaved caspase-3 (CC-3,
196 Extended Data Fig. 8), a well-established marker for apoptosis. As expected by the
197 earlier experiments, we found 50 % reduction of PV^+/CC-3^+ interneurons at p10
198 suggestive of strongly reduced apoptosis of PV^+ interneurons in the mutant mPFC
199 (Extended Data Fig. 8). Obviously, OPCs receive GABAergic input through $GABA_BR$
200 and send back pro-apoptotic signals to interneurons.

201 To confirm the selective cell death of interneurons, we induced the cKO as early as p1
202 and p2 and compared the apoptosis of inhibitory neurons with that of excitatory ones
203 at p5 and p7 (Fig. 3a). Interneuron apoptosis persists from p1 till p15 with a peak at p7
204 [7], while the time window for excitatory neuron apoptosis is rather narrow, between p2-
205 5 [30]. Apoptosis of total interneurons ($GAD67^+CC\text{-}3^+$) as well as PV interneurons

206 (PV$^+$CC-3$^+$ left panel in Fig. 3b) was significantly reduced in cKO mPFC at p5 and p7
207 (Fig. 3c), while that of the excitatory neurons (CTIP$^+$CC-3$^+$, right panel in Fig. 3b;
208 TBR1$^+$CC-3$^+$) did not change at both time points (Fig. 3c, Extended Data Fig. 9).
209 Therefore, we concluded that OPCs send pro-apoptotic signals back to interneurons
210 at the early postnatal weeks.

211 To molecularly identify the critical apoptotic factor released by OPCs, we first tested
212 the expression levels of several peptides which had been associated with cell survival
213 or cell death in ctl and cKO mPFC (Extended Data Fig. 10). Gene deletion was induced
214 at p1/2, and mPFC was collected at p7, the peak of interneuron apoptosis (Extended
215 Data Fig. 10). We found only the expression of the cytokine tumor necrosis factor-like
216 weak inducer of apoptosis (TWEAK, also known as Apo3l or TNF superfamily member
217 12, TNFSF12) to be diminished about 30 % in cKO mPFC (Fig. 3d, Extended Data
218 Fig. 10). TWEAK induces an apoptotic cell death after binding to its cognate TWEAK
219 receptor (TWEAKR; TNF Receptor Superfamily Member 12A, TNFRSF12A; also
220 known as FN14) [31]. Subsequently, we tested MACS-sorted OPCs (collected from cKO
221 and ctl cortices at p7) (Fig. 3d) as well as Oli-neu cells (an OPC cell line) treated with
222 $GABA_BR$ antagonist CGP 55845 for TWEAK. Also here, we observed TWEAK
223 downregulation (Extended Data Fig. 10). Three independent experiments, including
224 genetic deletion or pharmacological block of OPC $GABA_BR$ decreased TWEAK
225 expression (Fig. 3d, Extended Data Fig. 10).

226 To confirm that OPC-derived TWEAK can indeed induce neuronal apoptosis, we
227 treated primary cortical neurons with conditioned medium obtained from OPC Oli-neu
228 cultures (Fig. 3e). A selective TWEAKR antagonist, L524-0366 was added to the
229 conditioned medium at 20 μM to block the binding of TWEAK on interneurons
230 (Fig. 3e, f). While the conditioned medium from the OPC cell line increased interneuron
231 apoptosis (Fig. 3g, h), co-treatment with the TWEAKR antagonist prevented the cell

232 death. These results further substantiate that OPCs induces interneuron apoptosis via
233 TWEAK secretion.

234 In summary, our results demonstrate that OPCs induce interneuron apoptosis by
235 releasing TWEAK upon $GABA_BR$ activation. Blocking this pathway prevents the
236 apoptosis of interneurons. The concomitant dysregulation of interneuron density
237 results in a reduced inhibitory GABAergic tone and altered myelination in the mPFC.

238

239 *Interrupted OPC-interneuron communication after $GABA_BR$ loss in OPCs during*
240 *development generates cognitive impairment in adulthood*

241 The mPFC is responsible for cognitive processes and their regulatory finetuning is
242 guaranteed by the E/I balance [32]. To test whether the selectively reduced interneuron
243 apoptosis and the associated structural myelin alterations can generate defects in
244 neural circuits and cognition, we further performed *in vivo* investigations using
245 electrophysiology and behavioral analysis in 9w old animals after gene ablation was
246 induced at P7/8 (Fig. 4a).

247 The patch-clamp recordings described above had revealed a reduced firing rate of
248 interneurons suggesting an imbalance of E/I in the mutant mPFC (Fig. 2c, d). Impaired
249 cortical network activity of the mutant mice was also detected in
250 electroencephalographical (EEG) recordings. The power of the gamma wave,
251 especially the lower gamma wave band (30-50 Hz) was slightly, but significantly
252 decreased by about 10% in cKO mice (Fig. 4b).

253 To evaluate the impact of circuit dysregulation in the mutant mPFC for the living animal,
254 we challenged mice for their cognitive performance employing tasks of social cognitive
255 behavior which had been associated with proper mPFC function, i.e. social novelty and
256 new object recognition [33]. In addition, nest building behavior is often introduced as a
257 gauge of general well-being of the mice and also being an early sign of cognition

258 decline [34]. We observed that the mutant mice built significantly poorer nests with less
259 than half score of the control animal nests, indicating putative cognition deficits of the
260 mutant mice (Fig. 4c). The three-chamber test was used to assess social cognition by
261 analyzing mice for a form of general sociability and their interest in social novelty
262 (Fig. 4d). First, the three-chamber test was used to monitor general social behavior,
263 i.e. preference of other mice over objects. Both, ctl and cKO mice exhibited more
264 interest in the mouse rather than the object during the first test phase, indicating no
265 disorder in sociability of the mutant mice (Fig. 4e, Extended Data Fig. 11). At the
266 second phase, a social novelty preference was assessed. Control animals investigated
267 the unfamiliar mouse more than the familiar one, while the cKO mice exhibited no novel
268 social preference as they spent similar time in both chambers (Fig. 4f, Extended Data
269 Fig. 11). Employing a new object recognition test (Fig. 4g), we again observed the
270 cognition defect of cKO mice. Control animals were able to distinguish the new object
271 replaced after a 40 min break from the habituation, while the cKO mice showed similar
272 interest to both of the old and new objects (right panel in Fig. 4g-i). Open field test
273 showed that the motor activity of the cKO mice (in terms of the speed and total distance)
274 was not affected (Fig. 4j-l).

275 Hence, we conclude that $GABA_BRs$ of OPCs are essential for cognition by modifying
276 inhibitory circuits in the mPFC.

277

278 **Discussion**

279 A balance of excitation and inhibition (E/I) in the medial prefrontal cortex (mPFC) is of
280 key importance for mammalian cognition. Establishing correct cell densities and
281 subsequent myelination have been identified as pivotal elements during CNS
282 development [6, 17]. This has been well documented for fast-spiking parvalbumin-positive
283 (PV^+) interneurons. Here, we highlight OPCs as indispensable regulators of
284 interneuron population and myelination in the mPFC by providing a molecular
285 explanation and demonstrating how impaired bidirectional OPC-interneuron signaling
286 affects social cognitive behavior. OPCs at the first two postnatal weeks release
287 TWEAK to regulate interneuron apoptosis. Genetic ablation of $GABA_BR$ in OPCs at
288 the first postnatal week promoted interneuron survival. However, these neurons
289 displayed hypoactivity, less contacts with OPCs during development and deteriorated
290 myelin structures in the adulthood. Notably, these mutant mice exhibited severe
291 cognitive defects in their social behavior.

292 During development, large populations of immature interneurons invade the cortex
293 where their cell density is adjusted by programmed cell death [9, 10]. For assuring their
294 survival, these neurons form connections with adjacent cells and receive retrograde
295 signals from their targets [10, 11]. Interneuron apoptosis drastically increases at p7 [7],
296 shortly after formation of interneuron-OPC synapses at p4-5 [12]. Based on this
297 established knowledge, we hypothesized that OPCs could exert an apoptotic impact
298 to their presynaptic partners. Indeed, our data provide strong evidence that, starting
299 from postnatal day 5 on, OPCs elicit an apoptotic cascade of adjacent interneurons to
300 adjust their density. In OPCs, the regulatory process employs a $GABA_BR$-TWEAK
301 signaling pathway. TWEAK, TNF super family member 12 (TNFSF12), is TNF-like
302 weak apoptotic factor. Membrane-bound and cleaved isoforms of TWEAK are both
303 able to induce cell apoptosis by binding to the TWEAK receptor (TWEAKR, also known
304 as FN14) on the neuronal side [31, 35, 36]. According to our data $GABA_BR$-TWEAK

305 signaling preferentially affects interneurons, suggesting this 'kill me' signal acting
306 highly localized. Indeed, TWEAK is specifically recruited to synapses where
307 TWEAKRs are expressed [37]. OPCs directly sense GABAergic signals at their
308 interneuron-OPC synapse. Subsequent signaling triggers TWEAK expression and
309 translocation to the OPC surface, where it could directly bind interneuronal TWEAKRs.
310 Alternatively, the TWEAK ectodomain could be proteolytically cleaved and act as a
311 soluble factor. However, this scenario could also happen at soma-somatic contact sites
312 between OPCs and interneurons [38, 39]. The regulatory impact appears to be highly
313 specific since the OPC-induced interneuron apoptosis was restricted to the first two
314 postnatal weeks, a well-established time window of interneuron apoptosis [7, 30]. This
315 also explains why the cKO induction at the age of 4w did not impact OPC differentiation
316 and myelination, although $GABA_BR$ expression peaks in OPCs at 4w (data not shown).
317 Please note, instead of a gradual decline, we found a slight increase of PV^+CC3^+ cells
318 at p14 compared to p10, probably due to the age-dependent increase of PV expression
319 described for fast spiking interneurons [40].

320 Neuronal overpopulation is often accompanied with suppressed activity [6, 8]. In the
321 OPC-$GABA_BR$ cKO mice, we observed excessive number of PV^+ interneurons (about
322 30 % increase) while attenuated vGAT puncta (reduced to 80 %), suggesting single
323 PV^+ interneuron exhibits suppressed activity (about 60% ≈ 80 %÷130 %). This was
324 also shown by the sIPSP recording which was decreased to 60 % in the cKO mPFC.
325 Differentiation of oligodendrocytes and subsequent myelination are strongly affected
326 by neuronal activity [22, 26, 41]. Indeed, we observed a suppression of the inhibitory tone
327 in the mPFC at p10 followed by a change in oligodendrocyte density detected at p14.
328 Concomitantly, the oligodendrocytes formed less myelin (only 40 % of control scenario)
329 around the interneuronal axons and altered paranodal structures in the adult mPFC
330 which are essential for precise action potential propagation. Such reduction is
331 attributed to the restrained PV^+ neuron activity (60 %) and oligodendrocyte population

332 (74 %) (60 %×74 % ≈ 40 %). Regardless, the morphological deterioration was only
333 observed in the mPFC, but not in the corpus callosum composed axons of excitatory
334 neurons only [21]. In line with these neuron-type specific observations, the qRT-PCR
335 results indicated reduced levels of MBP, but not PLP mRNA expression in the mutant
336 mPFC, both at p14 and 9w of age. Axons of interneurons and excitatory neurons are
337 different in respect to the protein content of their myelin sheaths. MBP is preferentially
338 expressed in the myelin of inhibitory axons, while PLP is more prominent in excitatory
339 axons PLP [16].

340 An early loss of the $GABA_AR$ γ2 subunit in OPCs reduced the firing rate of presynaptic
341 PV^+ interneurons and caused a similar myelin defect of longer nodal structures in PV^+
342 neurons [4], the initially very different signal pathways of both, $GABA_AR$ and $GABA_BR$,
343 have to merge to affect myelin gene expression and OPC-axon contacts similarly. The
344 $GABA_AR$ signaling between interneurons and OPCs is relatively well established [4, 15,
345 42, 43]. E.g., the γ2 subunit of $GABA_AR$ contributes to the maintenance of the OPC, but
346 has no impact on oligodendrocyte formation [15]. However, the role of $GABA_BRs$ for OPC
347 differentiation is complex. We observed that $GABA_BR$ was essential for
348 oligodendrogenesis at the early development but not at later stages. Similary, an *in*
349 *vitro* study showed that activation of $GABA_BR$ by the selective agonist baclofen could
350 stimulate the differentiation of cortical OPCs prepared from p0-2 pups [14]. Since OPCs
351 are heterogeneous with age [44], $GABA_BR$ of OPCs could contribute to the
352 developmental diversity.

353 Obviously, the GABAergic signaling of OPCs plays pivotal roles for the myelination of
354 interneurons, which ensures precise finetuning of the local neural circuitry [45]. As seen
355 in chandelier cells [6], excessive number of interneurons in the OPC-$GABA_BR$ cKO mice
356 exhibited suppressed activity, and reduced myelination in the mPFC. All these
357 physiological and morphological abnormalities certainly contributed to cognition
358 impairment. A proper E/I ratio in the prefrontal cortex, especially early E/I balance in

359 mPFC, is extremely important for social cognition [32, 46]. When the pyramidal neuron
360 activity was enhanced in the mPFC at early p7-11 caused a severe cognitive
361 dysfunction in the adulthood [46]. In addition, despite relatively short axons, myelination
362 of cortical interneurons (mainly PV^+ neurons [16]) contributes significantly to the
363 finetuning of local activity in the mPFC and cortex, insuring proper behavior
364 performance [4, 6, 17].

365 In conclusion, our study demonstrates that OPCs regulate inhibition in the mPFC via
366 $GABA_BR$/TWEAK signaling. During development, OPCs determine the density of
367 interneurons by adjusting their apoptosis. Subsequently, correct myelination of
368 interneurons, as an essential component of the network activity in the mPFC,
369 determines the cognition and social behavior.

370 **References**

371 1. Douglas, R.J. & Martin, K.A. Inhibition in cortical circuits. *Curr Biol* **19**, R398-402 (2009).
372 2. Bai, X., Kirchhoff, F. & Scheller, A. Oligodendroglial GABAergic Signaling: More Than
373 Inhibition! *Neurosci Bull* (2021).
374 3. Marín, O. Interneuron dysfunction in psychiatric disorders. *Nat Rev Neurosci* **13**, 107-
375 120 (2012).
376 4. Benamer, N., Vidal, M., Balia, M. & Angulo, M.C. Myelination of parvalbumin
377 interneurons shapes the function of cortical sensory inhibitory circuits. *Nat Commun* **11**, 5151
378 (2020).
379 5. Ferguson, B.R. & Gao, W.J. PV Interneurons: Critical Regulators of E/I Balance for
380 Prefrontal Cortex-Dependent Behavior and Psychiatric Disorders. *Front Neural Circuits* **12**, 37
381 (2018).
382 6. Wang, B.S.*, et al.* Retinal and Callosal Activity-Dependent Chandelier Cell Elimination
383 Shapes Binocularity in Primary Visual Cortex. *Neuron* **109**, 502-515.e507 (2021).
384 7. Southwell, D.G.*, et al.* Intrinsically determined cell death of developing cortical
385 interneurons. *Nature* **491**, 109-113 (2012).
386 8. Orduz, D.*, et al.* Developmental cell death regulates lineage-related interneuron-
387 oligodendroglia functional clusters and oligodendrocyte homeostasis. *Nat Commun* **10**, 4249
388 (2019).
389 9. Lim, L., Mi, D., Llorca, A. & Marín, O. Development and Functional Diversification of
390 Cortical Interneurons. *Neuron* **100**, 294-313 (2018).
391 10. Davies, A.M. Regulation of neuronal survival and death by extracellular signals during
392 development. *EMBO J* **22**, 2537-2545 (2003).
393 11. Oppenheim, R.W. Cell death during development of the nervous system. *Annu Rev*
394 *Neurosci* **14**, 453-501 (1991).
395 12. Vélez-Fort, M., Maldonado, P.P., Butt, A.M., Audinat, E. & Angulo, M.C. Postnatal
396 switch from synaptic to extrasynaptic transmission between interneurons and NG2 cells. *J*
397 *Neurosci* **30**, 6921-6929 (2010).
398 13. Orduz, D.*, et al.* Interneurons and oligodendrocyte progenitors form a structured
399 synaptic network in the developing neocortex. *Elife* **4** (2015).
400 14. Serrano-Regal, M.P.*, et al.* Oligodendrocyte Differentiation and Myelination Is
401 Potentiated via GABA. *Neuroscience* **439**, 163-180 (2020).
402 15. Balia, M., Benamer, N. & Angulo, M.C. A specific GABAergic synapse onto
403 oligodendrocyte precursors does not regulate cortical oligodendrogenesis. *Glia* **65**, 1821-1832
404 (2017).
405 16. Micheva, K.D.*, et al.* A large fraction of neocortical myelin ensheathes axons of local
406 inhibitory neurons. *Elife* **5** (2016).
407 17. Maas, D.A.*, et al.* Interneuron hypomyelination is associated with cognitive
408 inflexibility in a rat model of schizophrenia. *Nat Commun* **11**, 2329 (2020).
409 18. Huang, W.*, et al.* Novel NG2-CreERT2 knock-in mice demonstrate heterogeneous
410 differentiation potential of NG2 glia during development. *Glia* **62**, 896-913 (2014).
411 19. Kang, S.H., Fukaya, M., Yang, J.K., Rothstein, J.D. & Bergles, D.E. NG2+ CNS glial
412 progenitors remain committed to the oligodendrocyte lineage in postnatal life and following
413 neurodegeneration. *Neuron* **68**, 668-681 (2010).
414 20. Zhu, X.*, et al.* Age-dependent fate and lineage restriction of single NG2 cells.
415 *Development* **138**, 745-753 (2011).
416 21. Fame, R.M., MacDonald, J.L. & Macklis, J.D. Development, specification, and diversity
417 of callosal projection neurons. *Trends Neurosci* **34**, 41-50 (2011).
418 22. Stedehouder, J.*, et al.* Fast-spiking Parvalbumin Interneurons are Frequently
419 Myelinated in the Cerebral Cortex of Mice and Humans. *Cereb Cortex* **27**, 5001-5013 (2017).

420 23. Stedehouder, J.*, et al.* Local axonal morphology guides the topography of interneuron
421 myelination in mouse and human neocortex. *Elife* **8** (2019).
422 24. Zonouzi, M.*, et al.* Individual Oligodendrocytes Show Bias for Inhibitory Axons in the
423 Neocortex. *Cell Rep* **27**, 2799-2808.e2793 (2019).
424 25. Scala, F.*, et al.* Layer 4 of mouse neocortex differs in cell types and circuit organization
425 between sensory areas. *Nat Commun* **10**, 4174 (2019).
426 26. Mitew, S.*, et al.* Pharmacogenetic stimulation of neuronal activity increases
427 myelination in an axon-specific manner. *Nat Commun* **9**, 306 (2018).
428 27. Chaudhry, F.A.*, et al.* The vesicular GABA transporter, VGAT, localizes to synaptic
429 vesicles in sets of glycinergic as well as GABAergic neurons. *J Neurosci* **18**, 9733-9750 (1998).
430 28. Dani, A., Huang, B., Bergan, J., Dulac, C. & Zhuang, X. Superresolution imaging of
431 chemical synapses in the brain. *Neuron* **68**, 843-856 (2010).
432 29. Fang, W.Q.*, et al.* Overproduction of upper-layer neurons in the neocortex leads to
433 autism-like features in mice. *Cell Rep* **9**, 1635-1643 (2014).
434 30. Wong, F.K.*, et al.* Pyramidal cell regulation of interneuron survival sculpts cortical
435 networks. *Nature* **557**, 668-673 (2018).
436 31. Chicheportiche, Y.*, et al.* TWEAK, a new secreted ligand in the tumor necrosis factor
437 family that weakly induces apoptosis. *J Biol Chem* **272**, 32401-32410 (1997).
438 32. Grossmann, T. The role of medial prefrontal cortex in early social cognition. *Front Hum*
439 *Neurosci* **7**, 340 (2013).
440 33. Bicks, L.K., Koike, H., Akbarian, S. & Morishita, H. Prefrontal Cortex and Social
441 Cognition in Mouse and Man. *Front Psychol* **6**, 1805 (2015).
442 34. Neely, C.L.C., Pedemonte, K.A., Boggs, K.N. & Flinn, J.M. Nest Building Behavior as an
443 Early Indicator of Behavioral Deficits in Mice. *J Vis Exp* (2019).
444 35. Winkles, J.A. The TWEAK-Fn14 cytokine-receptor axis: discovery, biology and
445 therapeutic targeting. *Nat Rev Drug Discov* **7**, 411-425 (2008).
446 36. Brown, S.A., Ghosh, A. & Winkles, J.A. Full-length, membrane-anchored TWEAK can
447 function as a juxtacrine signaling molecule and activate the NF-kappaB pathway. *J Biol Chem*
448 **285**, 17432-17441 (2010).
449 37. Cheadle, L.*, et al.* Sensory Experience Engages Microglia to Shape Neural Connectivity
450 through a Non-Phagocytic Mechanism. *Neuron* **108**, 451-468.e459 (2020).
451 38. Mangin, J.M., Kunze, A., Chittajallu, R. & Gallo, V. Satellite NG2 progenitor cells share
452 common glutamatergic inputs with associated interneurons in the mouse dentate gyrus. *J*
453 *Neurosci* **28**, 7610-7623 (2008).
454 39. Boulanger, J.J. & Messier, C. Oligodendrocyte progenitor cells are paired with GABA
455 neurons in the mouse dorsal cortex: Unbiased stereological analysis. *Neuroscience* **362**, 127-
456 140 (2017).
457 40. Larsen, R., Proue, A., Scott, E.P., Christiansen, M. & Nakagawa, Y. The Thalamus
458 Regulates Retinoic Acid Signaling and Development of Parvalbumin Interneurons in Postnatal
459 Mouse Prefrontal Cortex. *eNeuro* **6** (2019).
460 41. Nagy, B., Hovhannisyan, A., Barzan, R., Chen, T.J. & Kukley, M. Different patterns of
461 neuronal activity trigger distinct responses of oligodendrocyte precursor cells in the corpus
462 callosum. *PLoS Biol* **15**, e2001993 (2017).
463 42. Balia, M.*, et al.* Postnatal down-regulation of the GABAA receptor γ2 subunit in
464 neocortical NG2 cells accompanies synaptic-to-extrasynaptic switch in the GABAergic
465 transmission mode. *Cereb Cortex* **25**, 1114-1123 (2015).
466 43. Passlick, S.*, et al.* Expression of the γ2-subunit distinguishes synaptic and
467 extrasynaptic GABA(A) receptors in NG2 cells of the hippocampus. *J Neurosci* **33**, 12030-12040
468 (2013).
469 44. Spitzer, S.O.*, et al.* Oligodendrocyte Progenitor Cells Become Regionally Diverse and
470 Heterogeneous with Age. *Neuron* **101**, 459-471.e455 (2019).

471 45. Arancibia-Cárcamo, I.L., *et al.* Node of Ranvier length as a potential regulator of
472 myelinated axon conduction speed. *Elife* **6** (2017).
473 46. Bitzenhofer, S.H., Pöpplau, J.A., Chini, M., Marquardt, A. & Hanganu-Opatz, I.L. A
474 transient developmental increase in prefrontal activity alters network maturation and causes
475 cognitive dysfunction in adult mice. *Neuron* (2021).

476

477 **Acknowledgement**

478 We thank Daniel Schauenburg for excellent animal husbandry and Frank Rhode,
479 Alexander Grissmer and Samantha Bechet for experimental assistance. We are also
480 grateful to Prof. Jaqueline Trotter (University of Mainz, Mainz, Germany) for providing
481 the Oli-neu cell line and Prof. Leda Dimou (University of Ulm, Ulm, Germany) for
482 sharing MACs sorting protocols of OPCs. This work was supported by grants from the
483 Deutsche Forschungsgemeinschaft (SPP 1757, SFB 894 to FK; FOR2289 to AS, FK,
484 SPP1757 Young Investigator grant to XB), EraNet-Neuron BrIE to FK and
485 HOMFORexzellent2017 program to XB.

486 **Author contributions**

487 XB initiated the project. LF, XB, NZ, LC, NH, CL and AS performed experiments. LF,
488 XB, NZ, LC and RZ analyzed data. BB, WH. HC and CM provided materials. XB and
489 FK designed and supervised the study and wrote the manuscript with comments of the
490 other authors.

491 **Competing interests**

492 The authors declare no competing interests.

493 **Figure legends**

494 **Figure 1. Ablation of $GABA_BRs$ in OPCs attenuates oligodendrocyte**
495 **differentiation and myelination of interneurons in the medial prefrontal cortex.**
496 ***a***, Genetic strategy and experimental schedule. ***b,*** Prefrontal cortex in coronal section
497 stained with PDGFRα. tdTomato$^+$ (tdT$^+$) cells indicate recombined cells. ***b_1***, ***b_2***,
498 magnified images of ctl and cKO medial prefrontal cortex (mPFC, highlighted in ***b***). ***c,***
499 Recombination efficiency of OPCs in ctl and cKO mPFC. (*ctl=4, cKO=5, unpaired t-*
500 *test*). ***d,*** Western blot analysis of $GABA_BR$ subunit 1 in MACs sorted OPCs from cortex.
501 (*ctl=3, cKO=3, unpaired t-test*). ***e,*** Exemplary images of Olig2, PDGFRα and CC1
502 immunostaining in adult ctl and cKO mPFC. ***f, g,*** Quantification of OPC and
503 oligodendrocyte cell densities in mPFC and corpus callosum (cc). (mPFC: *ctl=7,*
504 *cKO=8, cc: ctl=4, cKO=4, multiple t-tests)*. ***h,*** Quantification of the oligodendrocyte
505 proportion among the total lineage (mPFC: *ctl=4, cKO=4;* cc: *ctl=3, cKO=6, multiple t-*
506 *tests)*. ***i,*** Immunostaining of Caspr and MBP in ctl and cKO mPFC. ***j,*** Quantitative
507 analysis of paranode length in mPFC (*ctl=4, cKO=4, multiple t-tests*). ***k,*** Western blot
508 analysis of MBP expression in mPFC and cc. (*ctl=4, cKO=3, multiple t-tests*). ***l,***
509 Overview of coronal brain slices immunostained with parvalbumin (PV) and MBP
510 shows abundant PV$^+$ neurons are myelinated in mPFC. ***m,*** 3D reconstruction of
511 myelinated PV$^+$ axons in ctl and cKO mPFC using Imaris software. ***n,*** Relative volume
512 of MBP$^+$ myelin sheaths wrapping PV$^+$ axons (*normalized to ctl). (ctl=3, cKO=3,*
513 *unpaired t-test*). Scale bars in **b**=1 mm, **b_2, e**=10 μm, **i, m**=5 μm, **l**=200 μm.

514 **Figure 2. In OPC-$GABA_BR$ cKO mice impaired control of interneuronal density**
515 **and firing rate reduces oligodendrocyte differentiation and myelin gene**
516 **expression at the onset of myelination.** ***a,*** Experimental schedule for ***b-d***. ***b***,
517 Immonostaining (left) and quantification (right) of PV$^+$ neurons in the mPFC at the age
518 of 9 weeks (*ctl=5, cK=9, unpaired t-test*). ***c,*** Exemplary traces of sIPSCs and sEPSCs
519 recorded at the layer V of mPFC. ***d,*** Quantification of frequency and amplitude of

520 sIPSC and sEPSC *(sIPSC: ctl=15 cells from 4 mice, cKO=15 cells from 5 mice; sEPSC:*
521 *ctl=26 cells from 4 mice, cKO=21 cells from 5 mice, Mann Whitney test).* ***e,***
522 Experimental schedule for ***f-m***. ***f,*** 3D reconstruction of OPCs and vGAT by PDGFRα
523 and vGAT immunostaining in ctl and cKO mPFC at p10 using Imaris software. vGAT
524 was classified into two subgroups: magenta vGATs have < 20nm distance from OPC
525 surface while grey vGATs have > 20nm. ***g, h***, Density (***g***) and volume (***h***) of vGAT in
526 ctl and cKO mPFC. (*ctl=4, cKO=4; multiple t-tests*). ***i,*** Quantification of synaptic vGAT
527 (< 20nm) density per μm^2 of OPC surface. *(ctl=4, cKO=4, unpaired t-test*). ***j,***
528 Immunostaining of OPCs and oligodendrocytes with PDGFRα, Olig2 and CC1 in p14
529 mPFC. ***k, l***, Density of OPCs (***k***) and oligodendrocytes (***l***) in ctl and cKO mPFC at p10
530 and p14. (*p10 and p14: ctl=5, cKO=4; multiple t-tests*). ***m,*** Quantitative analysis of MBP
531 mRNA level in ctl and cKO mPFC at p14. (*ctl=4, cKO=4, unpaired t-test)*. Scale bars
532 in **b**=50 μm, **f**=5 μm, **j**=10 μm.

533 **Figure 3. During early CNS development the apoptosis of supernumerous**
534 **interneurons is mitigated upon impaired release of TWEAK from $GABA_BR$-**
535 **deficient OPC.** ***a,*** Scheme of experimental plan. ***b,*** Representative images of
536 excitatory (CTIP) and inhibitory (PV^+) neurons co-stained with apoptotic marker CC-3
537 in p5 and p7 mPFC. ***c,*** Quantification of apoptotic neurons ($CC\text{-}3^+$) co-expressing
538 interneuron marker GAD67 and PV or excitatory neuronal marker CTIP and TBR1.
539 *(GAD67: p5-ctl=3, p5-cKO=4; p7-ctl=3, p7-cKO=5) (PV: p5-ctl=5, p5-cKO=3; p7-ctl=3,*
540 *p7-cKO=5) (CTIP: p5-ctl=7, p5-cKO=4; p7-ctl=9, p7-cKO=3) (TBR1: p5-ctl=4, p5-*
541 *cKO=4; p7-ctl=4, p7-cKO=4) (multiple t-tests)*. ***d,*** Relative mRNA level of TWEAK in
542 the mPFC and MACs-OPCs from ctl and cKO mice *(tissue-ctl=4, tissue-cKO=6; MACs-*
543 *ctl=4, MACs-cKO=3; multiple t-test).* ***e,*** Experimental design for *in vitro* studies. ***f,***
544 Immunolabeling of TWEAK receptor on 14 DIV PV^+ interneurons. ***g,*** Immunostaining
545 of apoptotic primary PV^+ neurons treated with conditional medium of Oli-neu cells co-
546 treated with or without TWEAKR antagonist L524-0366 (20 μM). ***h,*** Percentage of
547 apoptotic PV^+ neurons among total PV^+ neurons after the treatments *(n=3 independent*

548 *experiments, one-way ANOVA, multiple comparison)*. Scale bars in **b**=5 μm, **f**=20 μm,
549 **g**=50 μm.

550 **Figure 4. In OPC-GABA$_B$R cKO mice perturbed electrical activity translates into**
551 **deficits of social behavior.** ***a,*** Scheme of experimental plan. ***b,*** Representative
552 diagram of lower gamma band acquired by ECoG recordings. Violin plot shows
553 decreased gamma oscillation in the cKO mouse brain. (*ctl=24 from 4 mice, cKO=24*
554 *from 4 mice, unpaired t-test*). ***c,*** Impaired nest building ability of mutant mice. (*ctl=9,*
555 *cKO=10, Mann Whitney test*). ***d***, Scheme of three-chamber behavior test. ***e,***
556 Quantification of the sniffing time with mouse (***e***) or with unfamiliar mouse (***f***) among
557 total sniffing time (*ctl=9, cKO=9, unpaired t-tests*). ***g,*** Scheme of new object recognition
558 test. ***h,*** Assessment of object preference *(ctl=10, cKO=10)*. ***i,*** Percentage of sniffing
559 time with new object among total sniffing time. *(ctl=10, cKO=10, upaired t-test*). ***j,***
560 Representative trajectory charts of the animals during the open field test. ***k, l,*** Both ctl
561 and cKO mice exhibited similar motor activities shown by the speed and distance
562 analysis. (*ctl=10, cKO=14, unpaired t-tests).*

563

564 **Supplementary figure legends**

565 **Supplementary Fig.1. OPC and oligodendrocyte density is not altered in the**
566 **corpus callosum of mutant mice. a,** Scheme of experimental schedule (left panel)
567 and analyzed brain region in highlight, i.e. corpus callosum (cc, right panel). **b,** Corpus
568 callosal OPCs and oligodendrocytes of ctl and cKO mice were immunolabeled with
569 PDGFRα and CC1 respectively at the age of 2w and 9w. Olig2 was used as lineage
570 marker and tdTomato was indicator of recombined cells. **c,** OPC recombination
571 efficiency in ctl and cKO cc (*ctl=86.22±0.57 (n=3), cKO=76.17±3.10 (n=6*), unpaired t-
572 test). **d, e,** Cell density of OPCs (PDGFRα$^+$) and oligodendrocytes (CC1$^+$) in cc of 2w-
573 and 9w-old mice were not changed. OPC: (*2w-ctl=77.02±4.21 (n=8), 2w-cKO=80±4.72*
574 *(n=8), unpaired t-test*) (*9w-ctl=30.01±3.68 (n=4), 9w-cKO=27.56±2.26 (n=4), unpaired*
575 *t-test*); oligodendrocytes (*2w-ctl=121.70±12.31 (n=8), 2w-cKO=97.62±10.54 (n=8),*
576 *unpaired t-test*) (*9w-ctl=296.90±32.83 (n=4), 9w-cKO=300.30±28.47 (n=4), unpaired*
577 *t-test*). **f,** Percentage of oligodendrocytes among total Olig2$^+$ cell population,
578 considered as OPC differentiation rate, was not changed at both ages (*2w-*
579 *ctl=60.26±3.61(n=8), 2w-cKO=53.98±3.73 (n=8), unpaired t-test*) (*9w-ctl=92.37±0.12*
580 *(n=3), 9w-cKO=91.33±0.69 (n=6), unpaired t-test*).

581 **Supplementary Fig.2. Parameters of myelination remain largely unaltered in the**
582 **corpus callosum of mutant mice. a,** Scheme of experimental schedule (left panel)
583 and analyzed brain region in highlight, i.e. mPFC and cc. **b,** Quantification of node
584 length of ctl and cKO mPFC. **c,** Paranode length is increased in the cKO mPFC. **d,**
585 Density of nodes remained same in the cKO mPFC. **e,** Relative mRNA level of MBP is
586 reduced in the cKO mPFC, while PLP mRNA is not affected (*ctl: n=4, cKO: n=3,*
587 *unpaired t-test*). **f,** Immunostaining of Caspr and MBP in cc of ctl and cKO mice. **g-i,**
588 Paranodal length and node density in ctl and cKO cc remained same. **j,** Electron
589 microscopic analysis of myelin ultrastructure in sagittal section of cc from ctl and cKO
590 mice. **k, l,** Quantification of g-ratios of axonal myelination shows unchanged

591 myelination in cKO cc. **m,** Compound action potential conduction velocity was not
592 altered indicated by patch clamp recordings. N1 indicates non-myelinated axonal
593 conduction velocity, while N2 is for myelinated axons.

594 **Supplementary Fig.3. Ablation of $GABA_BR$ in oligodendrocytes do not affect**
595 **formation and density of oligodendrocytes. a,** Scheme of transgene construction.
596 **b,** Experimental schedule. **c,** Overview of CC1 immunostaining in a sagittal section of
597 9w old ctl mouse. Extensive tdTomato distribution shows a high recombination in
598 different brain regions of transgenic mouse. **d,** Magnified images from prefrontal cortex
599 (yellow box in **c**) and corpus callosum (white box in **c**). **e,** Quantification of
600 oligodendrocyte recombination efficiency in PFC were identical, while cKO mice
601 showed smaller recombination efficiency in cc. However, density of oligodendrocyte
602 cells did not differ between ctl and cKO mice in both PFC and cc. arrows: recombined
603 oligodendrocyte; triangles: non-recombined oligodendrocyte.

604 **Supplementary Fig.4. Dense population of parvalbumin-expressing**
605 **interneurons in the adult mouse cortex. a,** Overview of coronal brain slices
606 immunostained with parvalbumin and MBP shows abundant PV^+ neurons in the
607 somatosensory cortex. **b,** Magnified view (yellow box in **a**) shows the absence of PV^+
608 axons in the corpus callosum.

609 **Supplementary Fig.5. At the onset of myelination, $GABA_BR$-deficient OPCs**
610 **receive less GABAergic input in the mPFC mutant mice. a,** Experimental timeline
611 and analyzed brain region (mPFC) in highlight.**b,** Immunostaining of PDGFRα and
612 vGAT in the mPFC of p10 mice. **c,** Quantitative analysis of vGAT volume and the
613 distance to OPC surface (*ctl: n=4, cKO: n=4*). **d,** The volume of vGAT in cKO mPFC
614 was smaller than that in ctl group.

615 **Supplementary Fig.6. The differentiation of $GABA_BR$-deficient OPCs is**
616 **suppressed in the mutant mPFC. a,** Scheme of experimental schedule and analyzed

617 brain region (mPFC). **b,** Recombination efficiency of OPCs (% of $P\alpha^+tdt^+/P\alpha^+$) at p14
618 is identical in the ctl and cKO mPFC. **c,** Immunostaining and quantification of OPCs
619 incorporated with BrdU shows no change in OPC proliferation in the cKO mPFC at p14
620 (*ctl: n=4, cKO: n=5, unpaired t-test*). **d,** Immunostaining and quantification of
621 oligodendrocytes incorporated with BrdU shows decreased OPC differentiation in the
622 cKO mPFC at p14 (*ctl: n=4, cKO: n=5, unpaired t-test*). **e,** The portion of
623 oligodendrocytes among the oligodendrocyte lineage declined in cKO mPFC at p14
624 (*ctl: n=5, cKO: n=4, unpaired t-test*).

625 **Supplementary Fig.7. Controlled ablation of $GABA_BR$ in OPCs of young adult**
626 **mice does not affect oligodendrogenesis. a,** Scheme of experimental schedule and
627 the analyzed brain regions (mPFC and cc). **b,** Immunostaining of OPCs (PDGFRα)
628 and oligodendrocyte (CC1) with Olig2 (lineage marker) at ctl and cKO mouse mPFC
629 and cc at the age of 9w. **c, d,** Cell densities of OPCs ($PDGFR\alpha^+$) and oligodendrocytes
630 ($CC1^+$) of cKO animals were the same as those for ctl mice in both mPFC and cc.
631 mPFC. *($PDGFR\alpha^+$: (ctl=17.58±0.53 (n=4), cKO=18.69±1.58 (n=2), unpaired t-test));*
632 *($CC1^+$: (ctl=9.05±1.38 (n=4), cKO=7.95±1.40 (n=2), unpaired t-test));* cc: *($PDGFR\alpha^+$:*
633 *(ctl=35.38±2.25 (n=4), cKO=32.37±4.81 (n=2), unpaired t-test)); ($CC1^+$:*
634 *(ctl=311.81±43.39 (n=4), cKO=339.20±70.53 (n=2), unpaired t-test))*. **e,** The proportion
635 of oligodendrocyte among total lineage cells did not change, suggesting OPC
636 differentiation remained same in the mutant mouse mPFC and cc. mPFC:
637 *(ctl=30.49±5.13 (n=3), cKO=29.91±2.62 (n=2), unpaired t-test); cc: (ctl=89.52±1.30*
638 *(n=3), cKO=91.21±0.471 (n=2), unpaired t-test)*. **f,** MBP expression is not altered in
639 the cKO mPFC at mRNA level (*ctl: n=4, cKO: n=3, unpaired t-test*).

640 **Supplementary Fig.8. The apoptosis of interneurons is mitigated in the mPFC of**
641 **mutant mice at p14. a,** Timeline of experiments and scheme of analyzed brain region
642 mPFC in highlight. **b,** Immunostaining of PV^+ neurons with apoptotic marker (cleaved
643 caspase-3) at p10 of ctl and cKO mPFC. **c,** Quantification of apoptotic PV^+ neurons at

644 p10 and p14 shows reduced PV^+ neuronal apoptosis in the cKO mPFC compared to
645 ctl (p10*: ctl=2.03±0.47 (n=6), cKO=0.92±0.34 (n=3), unpaired t-test;* p14:
646 *ctl=3.70±1.21 (n=6), cKO=2.50±0.72 (n=9), unpaired t-test)*. **d,** Representative images
647 of apoptotic neurons at p14 of ctl and cKO mPFC. **e,** Quantification of apoptotic total
648 neurons ($NeuN^+CC\text{-}3^+$) at p14 *(ctl=2.76±0.42 (n=12), cKO=1.42±0.29 (n=9), unpaired*
649 *t-test)*.

650 **Supplementary Fig.9. Ablation of $GABA_BR$ expression in OPCs does not affect**
651 **the apoptosis or survival of excitatory neurons. a,** Scheme of experimental
652 schedule (left panel) and analyzed brain region in highlight. **b,** About 40 % of OPCs
653 are recombined (% of $PDGFR\alpha^+tdT^+/PDGFR\alpha^+$) at p7 both in the ctl and cKO mPFC.
654 **c, d,** Immunostainings and quantification of excitatory neurons ($TBR1^+$) with apoptotic
655 marker CC-3 in mPFC of ctl and cKO pups at p5 (**c**) and p7 (**d**) (p5: *ctl=1.64±0.39*
656 *(n=4), cKO=1.74±0.24 (n=4), unpaired t-test;* p10*: ctl=0.74±0.18 (n=4),*
657 *cKO=0.67±0.16 (n=4), unpaired t-test*).

658 **Supplementary Fig.10. TWEAK expression in OPCs is regulated by $GABA_BRs$. a,**
659 Scheme of experimental design. **b,** Relative mRNA level of cytokines in the mPFC of
660 ctl and cKO mouse at p7. *(TNF-α: ctl=1±0.34 (n=4), cKO=1.23±0.36 (n=6), unpaired t-*
661 *test); (TWEAK: ctl=1±0.10 (n=4), cKO=0.67±0.08 (n=6), unpaired t-test); (FasL:*
662 *ctl=1±0.57 (n=2), cKO=0.91±0.23 (n=4), unpaired t-test); (TNFSF7: ctl=1±1.00 (n=4),*
663 *cKO=0.93±0.67 (n=6), unpaired t-test); (Trp53: ctl=1±0.11 (n=4), cKO=1.14±0.08*
664 *(n=6), unpaired t-test); (NGF: ctl=1±0.24 (n=5), cKO=1.08±0.18 (n=6), unpaired t-test)*.
665 **c,** Western blot analysis of TWEAK expression in Oli-neu cells treated with
666 50 μM Baclofen at the presence or absence of 20 μM CGP 55845 (n=5 independent
667 experiments). The isoform in 36 KDa (blue box) was analyzed.

668 **Supplementary Fig.11. OPC-$GABA_BR$ cKO mice exhibit impaired social behavior.**
669 **a, b,** Mutant mice stayed longer at the chamber of mouse than object, indicating that

670 sociability of the mutant mouse is not affected. **c, d,** Mutant mice spent similar time at
671 the chambers of familiar and unfamiliar mouse, suggesting impaired cognition of the
672 cKO mice (*ctl (n=9), cKO (n=9), paired t-test*).

Figure 1

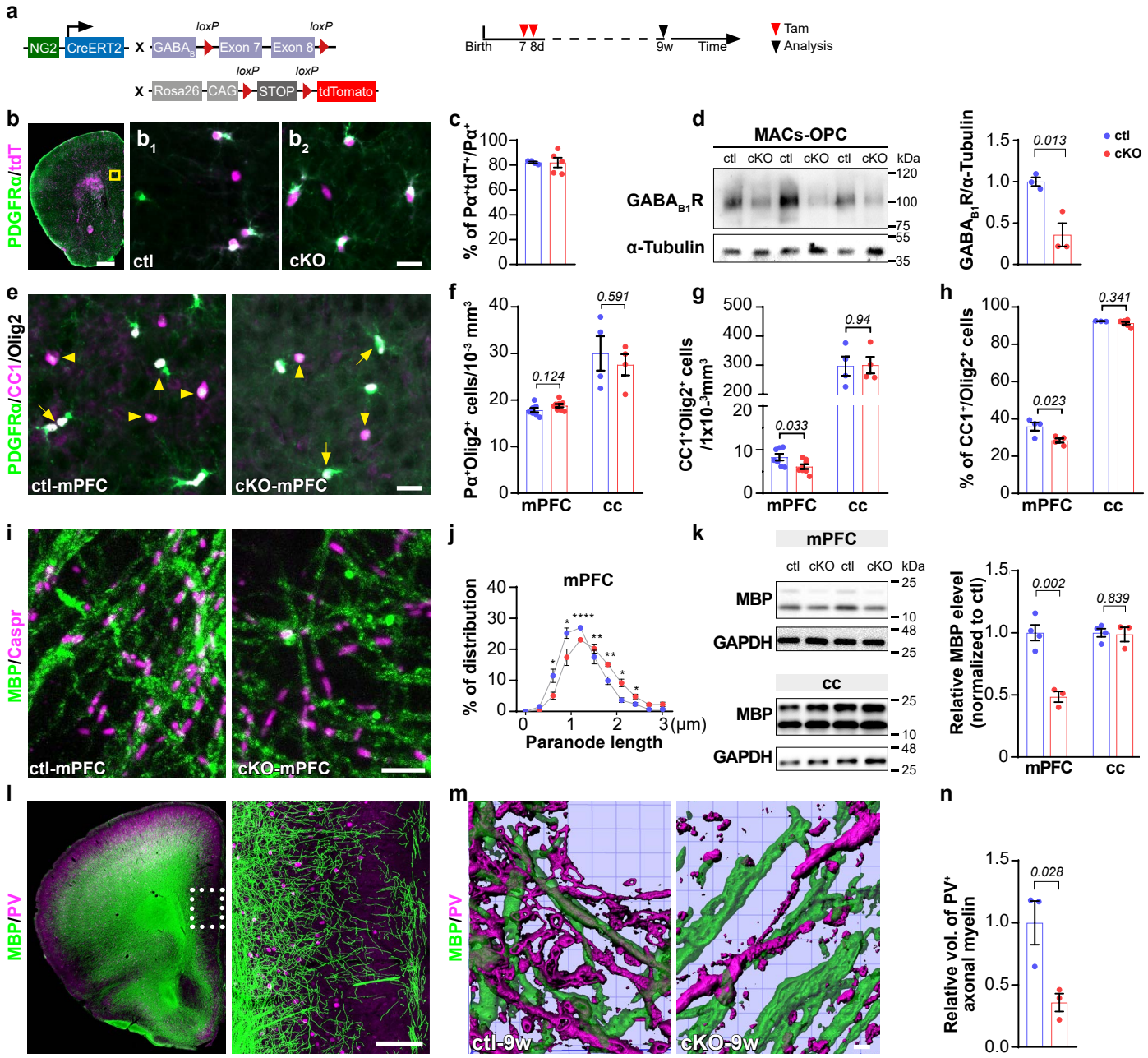
a
NG2
CreERT2
GABA
loxP
Exon 7
Exon 8
Rosa26
CAG
STOP
tdTomato
Birth
7 8d
9w
Time
Tam
Analysis
b
PDGFRα/tdT
ctl
cKO
c
% of Pα+tdT+/Pα+
d
MACs-OPC
ctl cKO ctl cKO ctl cKO
kDa
GABAB1R
α-Tubulin
GABAB1R/α-Tubulin
0.013
ctl
cKO
e
PDGFRα/CC1/Olig2
ctl-mPFC
cKO-mPFC
f
Pα+Olig2+ cells/10-3 mm3
0.124
0.591
mPFC
cc
g
CC1+Olig2+ cells /1x10-3mm3
0.033
0.94
h
% of CC1+/Olig2+ cells
0.023
0.341
i
MBP/Caspr
j
mPFC
% of distribution
Paranode length
(μm)
k
MBP
GAPDH
Relative MBP elevel (normalized to ctl)
0.002
0.839
l
MBP/PV
m
ctl-9w
cKO-9w
n
Relative vol. of PV+ axonal myelin
0.028

Figure 2

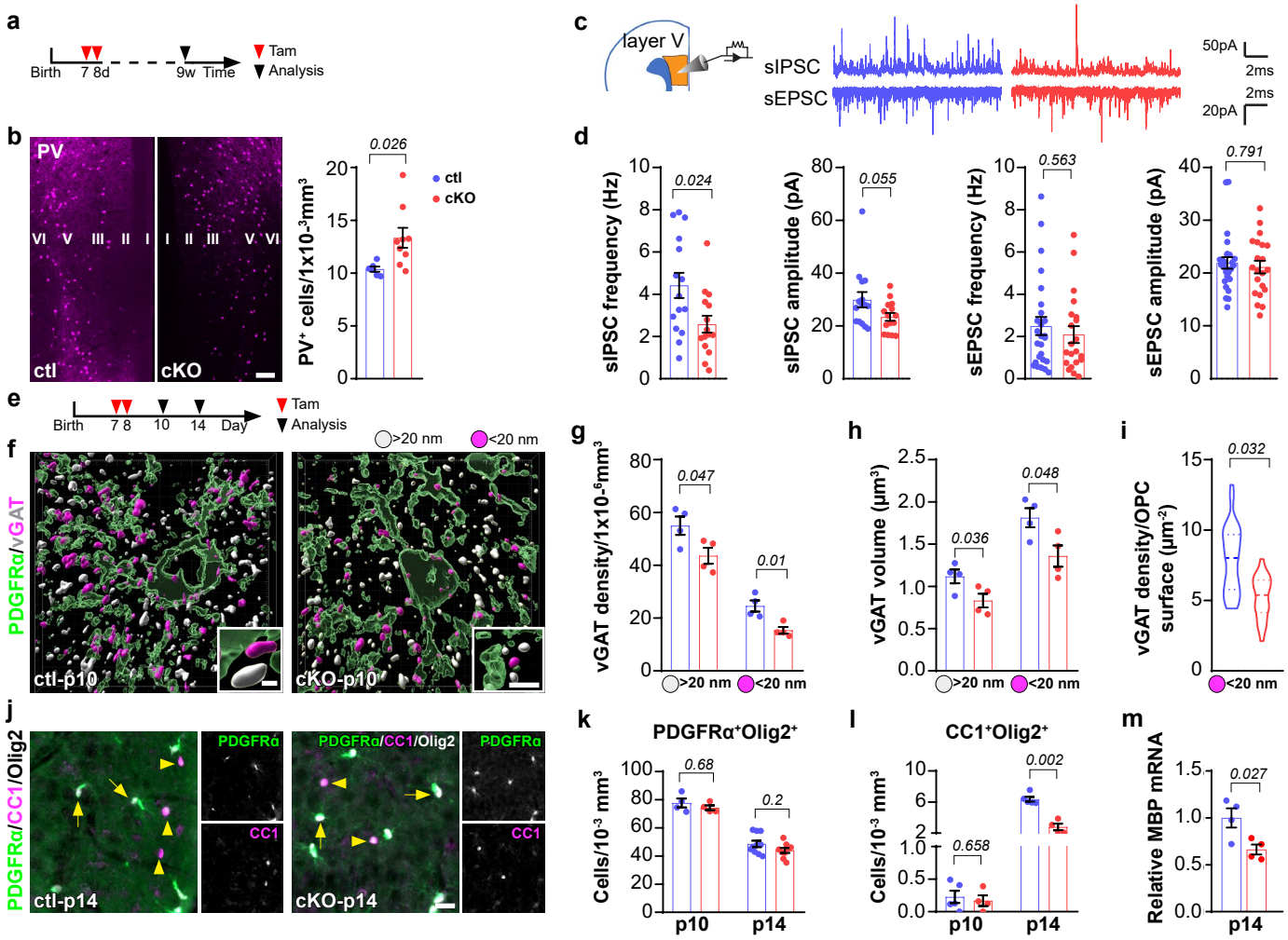
a
Birth
7 8d
9w Time
Tam
Analysis
b
PV
VI V III II I
I II III V VI
ctl
cKO
PV+ cells/1x10-3mm3
0.026
ctl
cKO
c
layer V
sIPSC
sEPSC
50pA
2ms
2ms
20pA
d
sIPSC frequency (Hz)
0.024
sIPSC amplitude (pA)
0.055
sEPSC frequency (Hz)
0.563
sEPSC amplitude (pA)
0.791
e
Birth
7 8
10
14
Day
Tam
Analysis
f
PDGFRα/vGAT
>20 nm
<20 nm
ctl-p10
cKO-p10
g
vGAT density/1x10-6mm3
0.047
0.01
>20 nm
<20 nm
h
vGAT volume (μm3)
0.036
0.048
>20 nm
<20 nm
i
vGAT density/OPC surface (μm-2)
0.032
<20 nm
j
PDGFRα/CC1/Olig2
PDGFRα
CC1
PDGFRα/CC1/Olig2
PDGFRα
CC1
ctl-p14
cKO-p14
k
PDGFRα+Olig2+
Cells/10-3 mm3
0.68
0.2
p10
p14
l
CC1+Olig2+
Cells/10-3 mm3
0.658
0.002
p10
p14
m
Relative MBP mRNA
0.027
p14

Figure 3

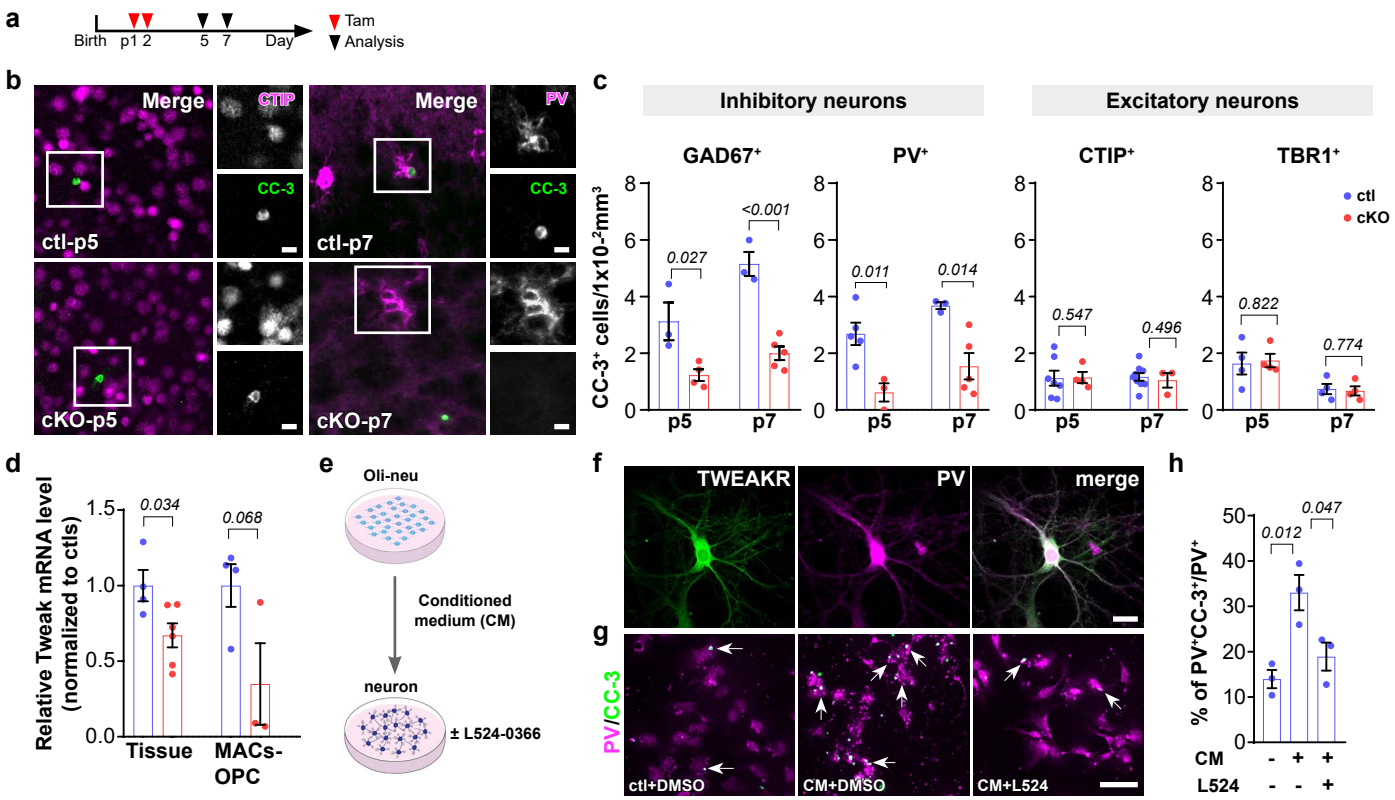
a
Birth
p1 2
5
7
Day
Tam
Analysis
b
Merge
CTIP
CC-3
ctl-p5
cKO-p5
Merge
PV
CC-3
ctl-p7
cKO-p7
c
Inhibitory neurons
Excitatory neurons
GAD67+
PV+
CTIP+
TBR1+
CC-3+ cells/1x10-2mm3
0.027
<0.001
0.011
0.014
0.547
0.496
0.822
0.774
p5
p7
ctl
cKO
d
Relative Tweak mRNA level (normalized to ctls)
0.034
0.068
Tissue
MACs-OPC
e
Oli-neu
Conditioned medium (CM)
neuron
± L524-0366
f
TWEAKR
PV
merge
g
PV/CC-3
ctl+DMSO
CM+DMSO
CM+L524
h
% of PV+CC-3+/PV+
0.012
0.047
CM
L524

Figure 4

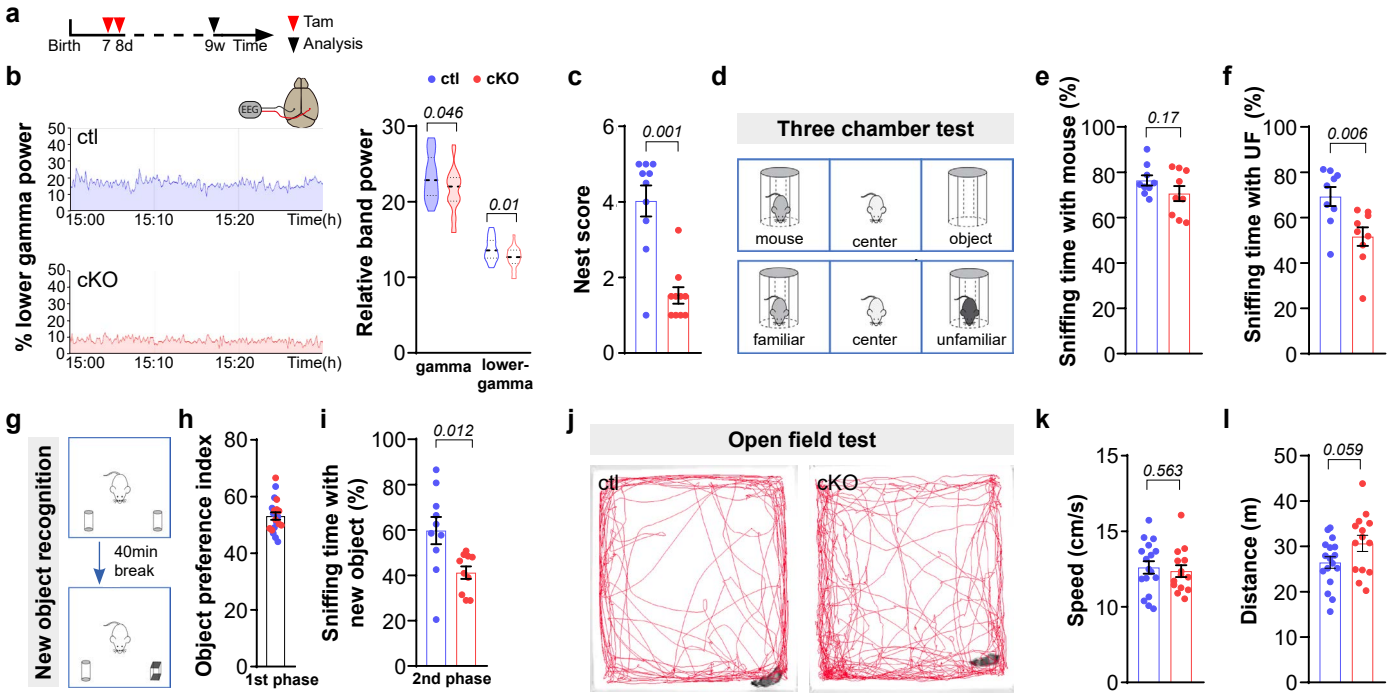
a
Birth
7 8d
9w
Time
Tam
Analysis
b
EEG
ctl
cKO
% lower gamma power
15:00
15:10
15:20
Time(h)
Relative band power
0.046
0.01
gamma
lower-gamma
c
Nest score
0.001
d
Three chamber test
mouse
center
object
familiar
center
unfamiliar
e
Sniffing time with mouse (%)
0.17
f
Sniffing time with UF (%)
0.006
g
New object recognition
40min break
h
Object preference index
1st phase
i
Sniffing time with new object (%)
0.012
2nd phase
j
Open field test
ctl
cKO
k
Speed (cm/s)
0.563
l
Distance (m)
0.059

Supplementary figure 1

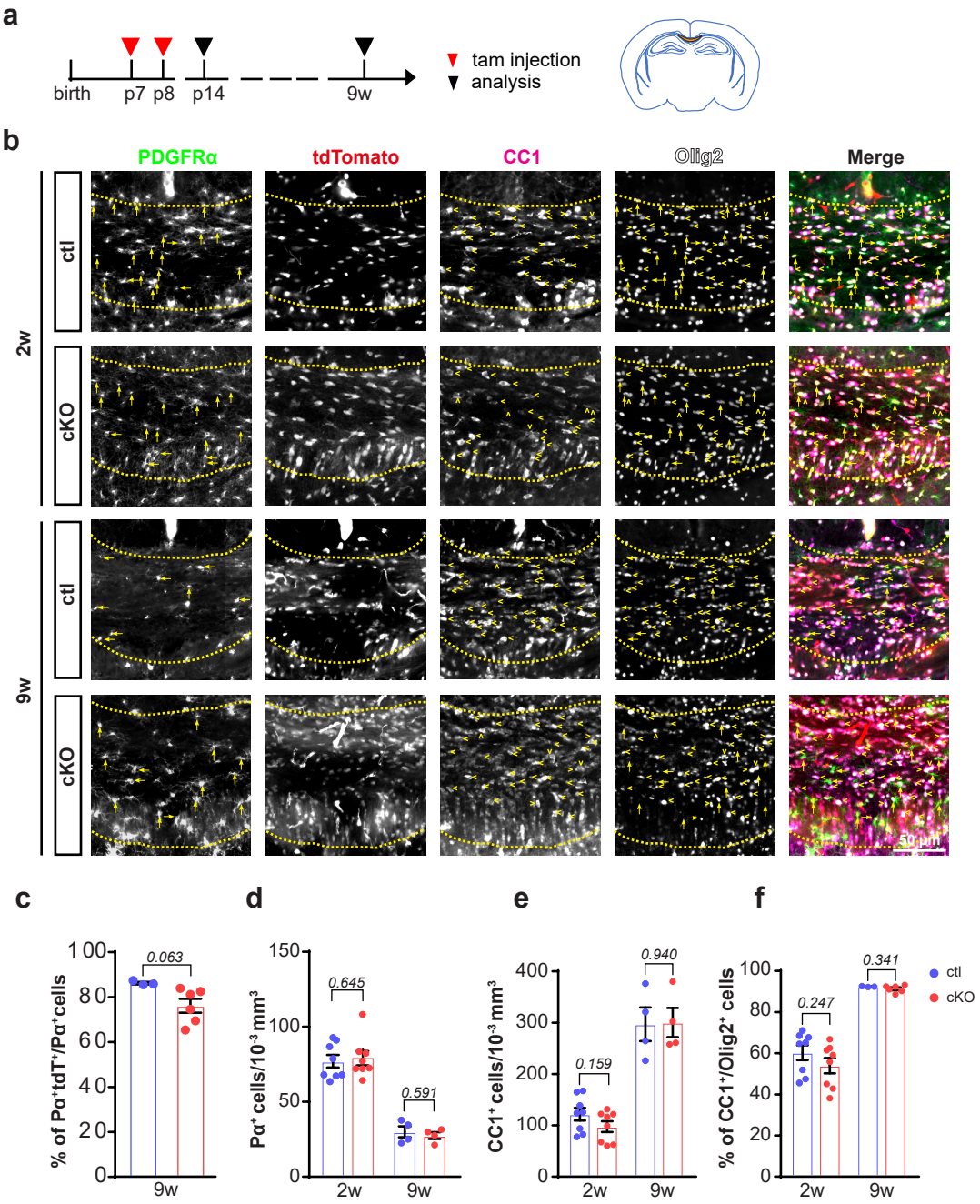

Supplementary figure 2

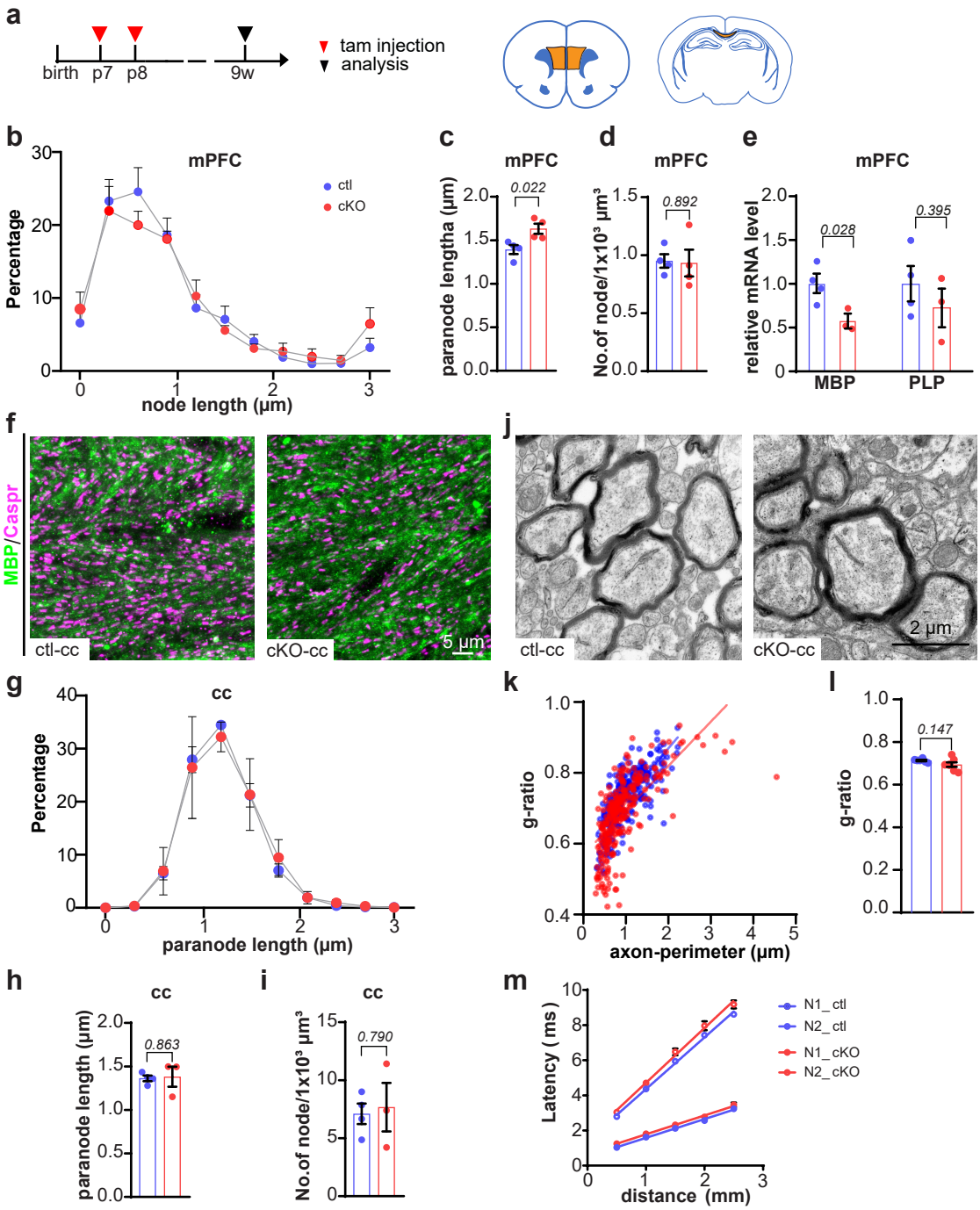

Supplementary figure 3

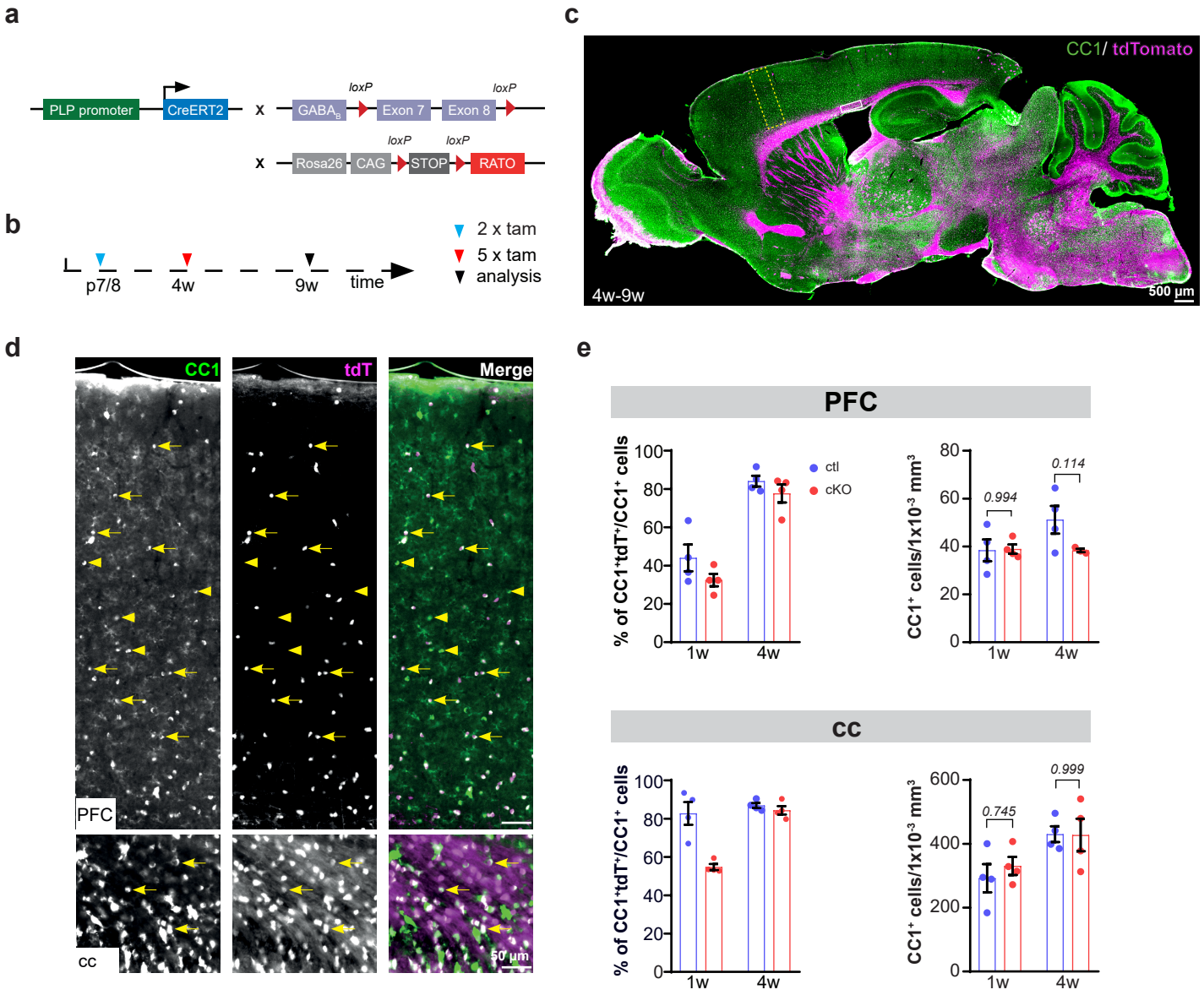

Supplementary figure 4

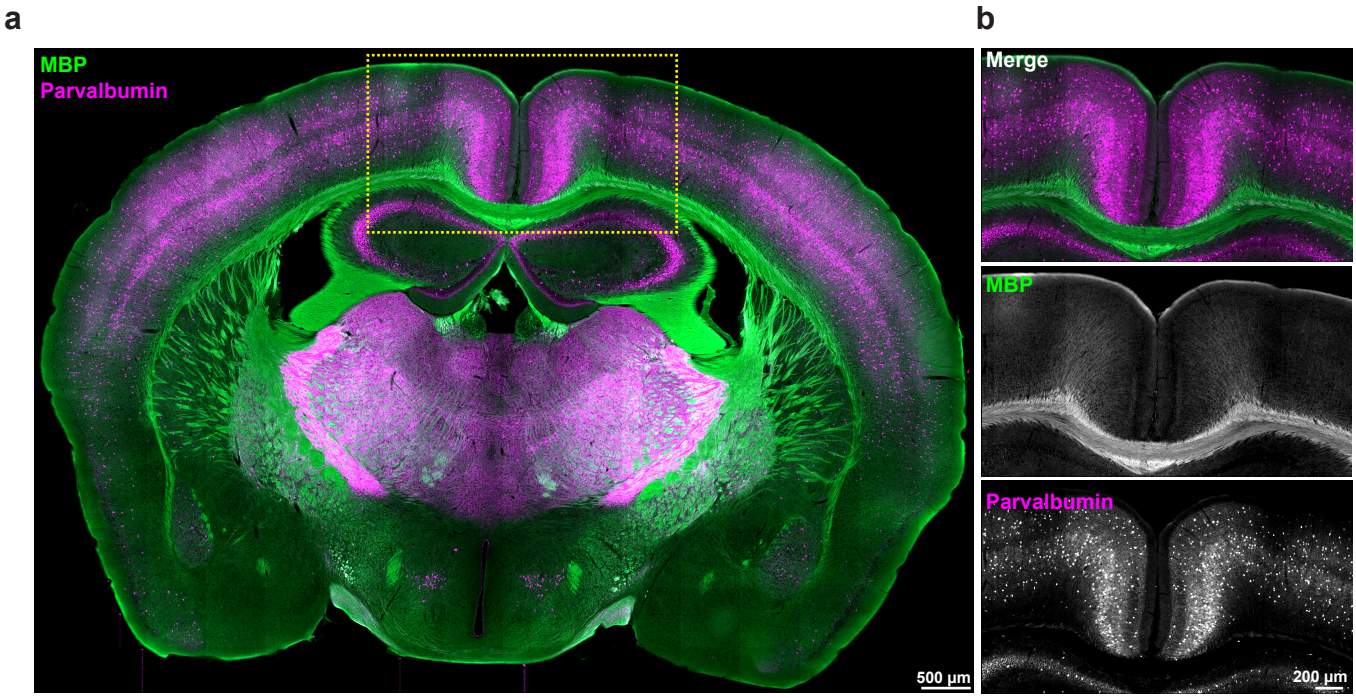

Supplementary figure 5

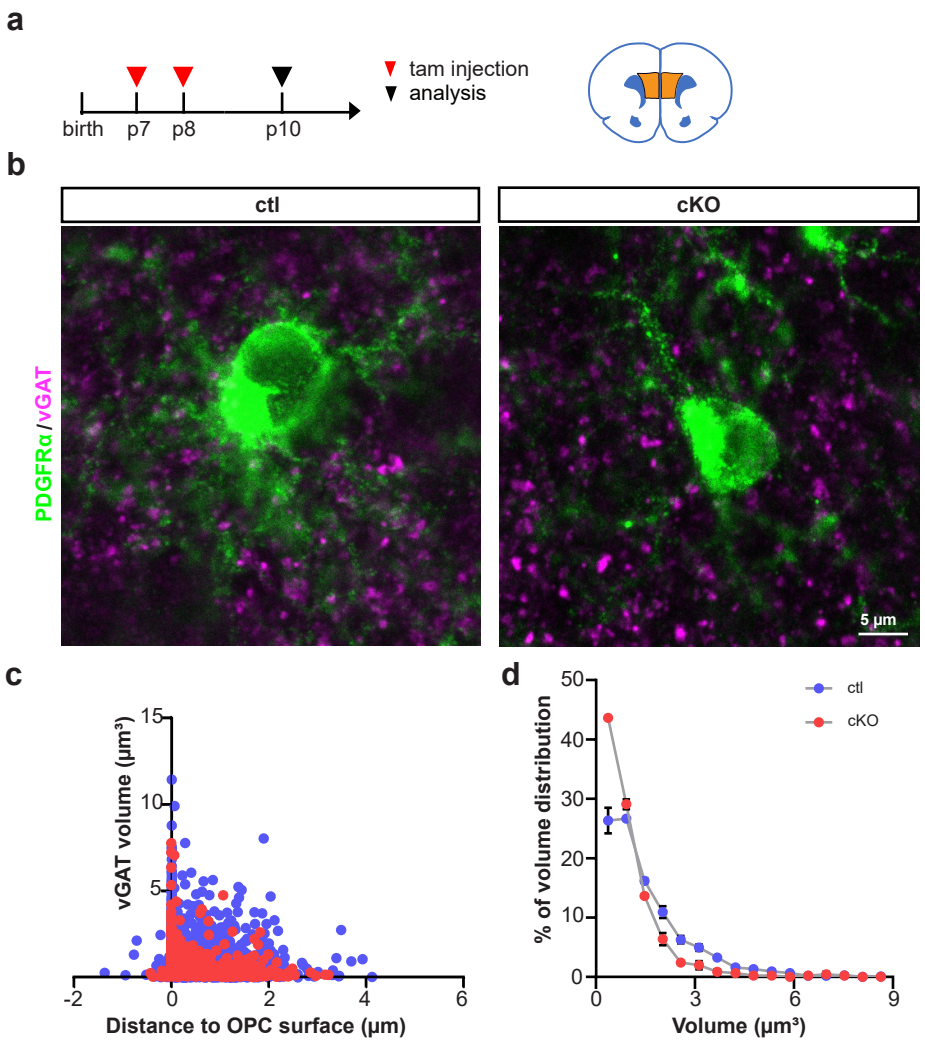

Supplementary figure 6

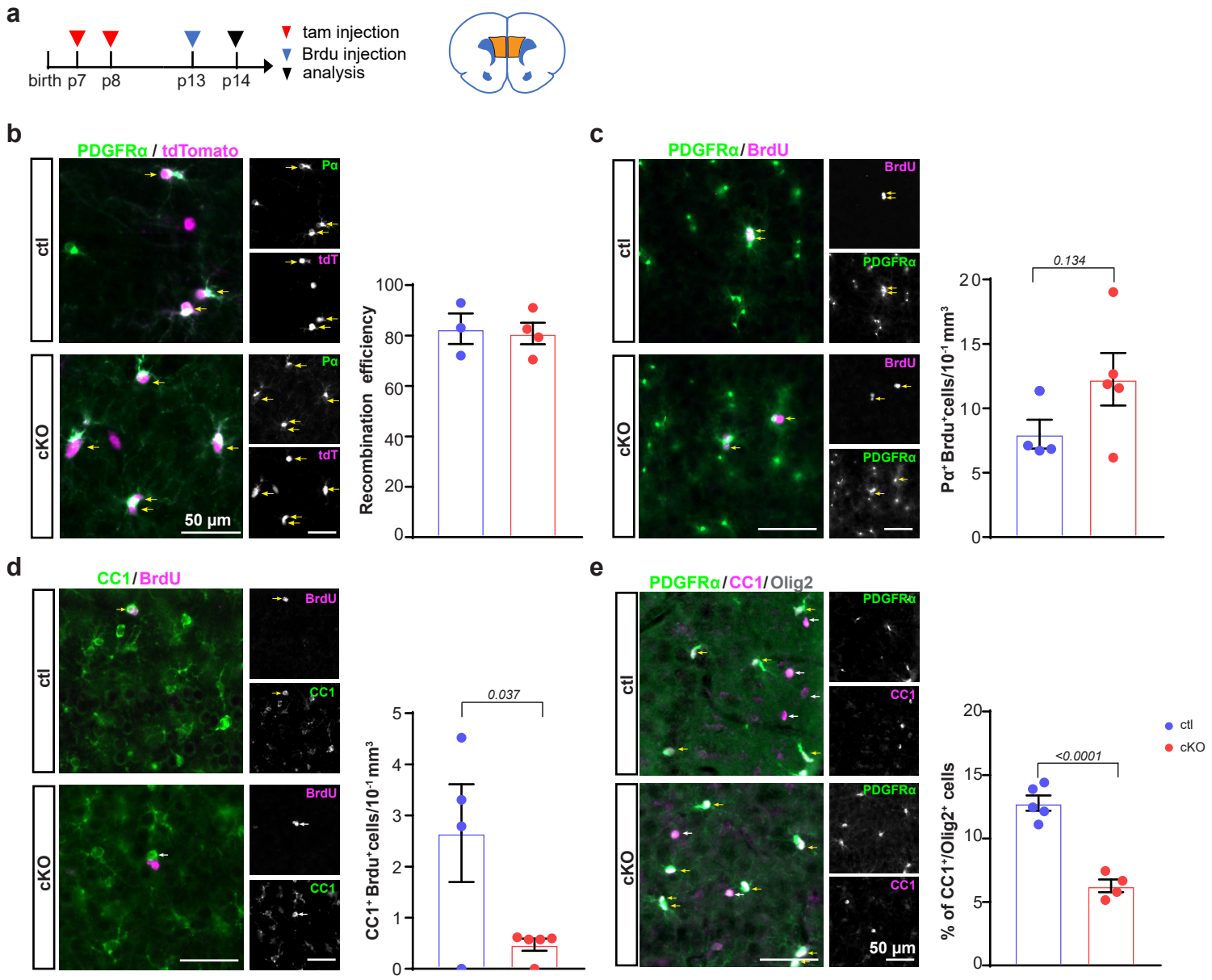

Supplementary figure 7

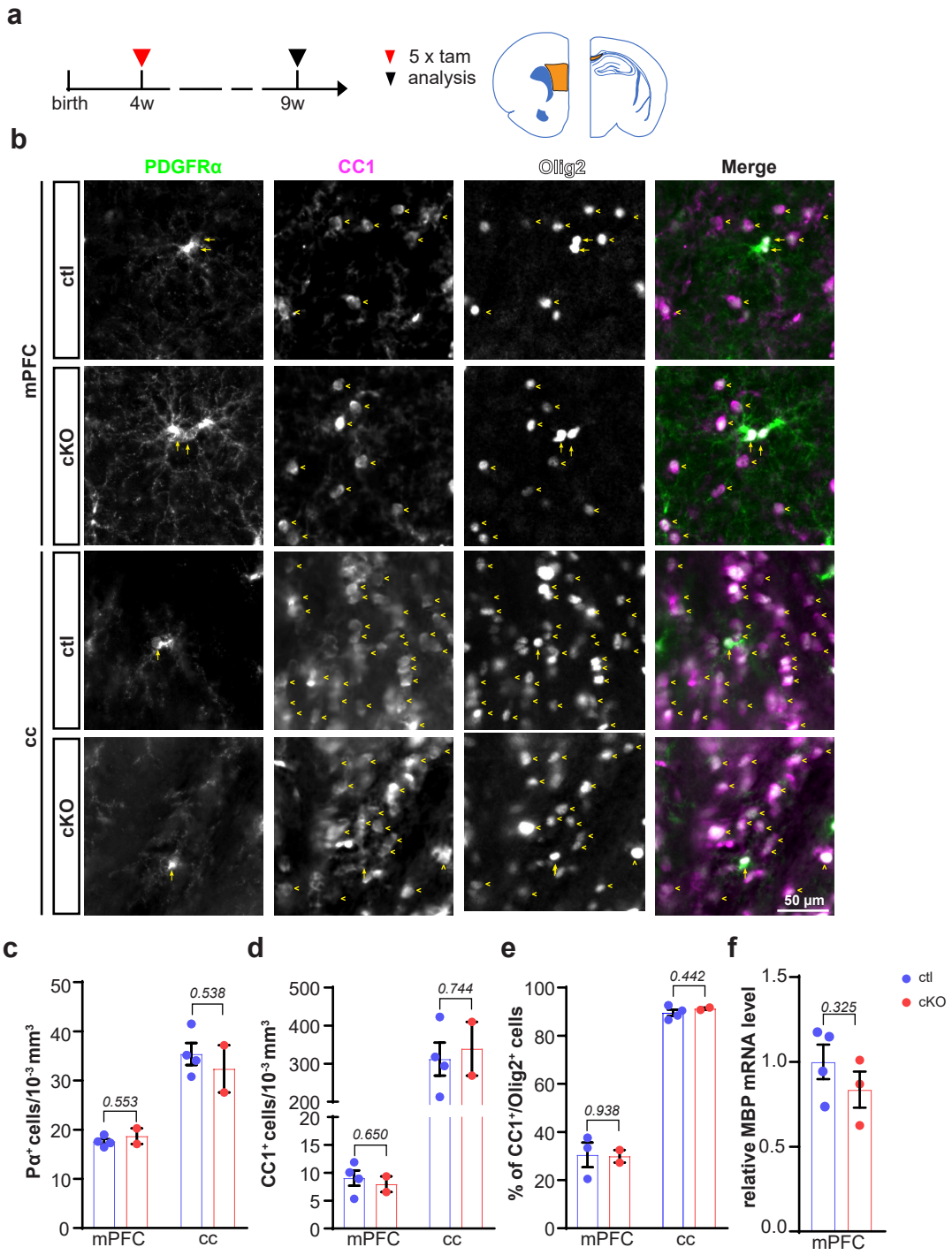

Supplementary figure 8

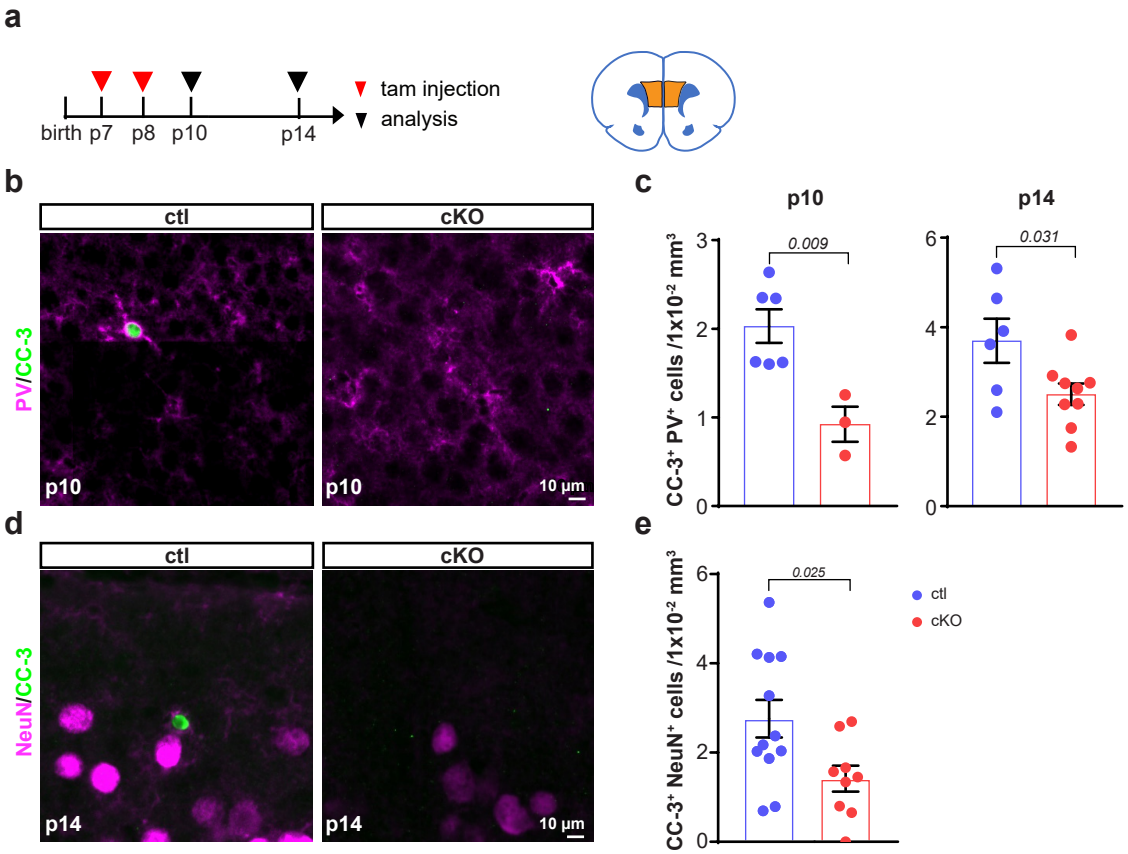

Supplementary figure 9

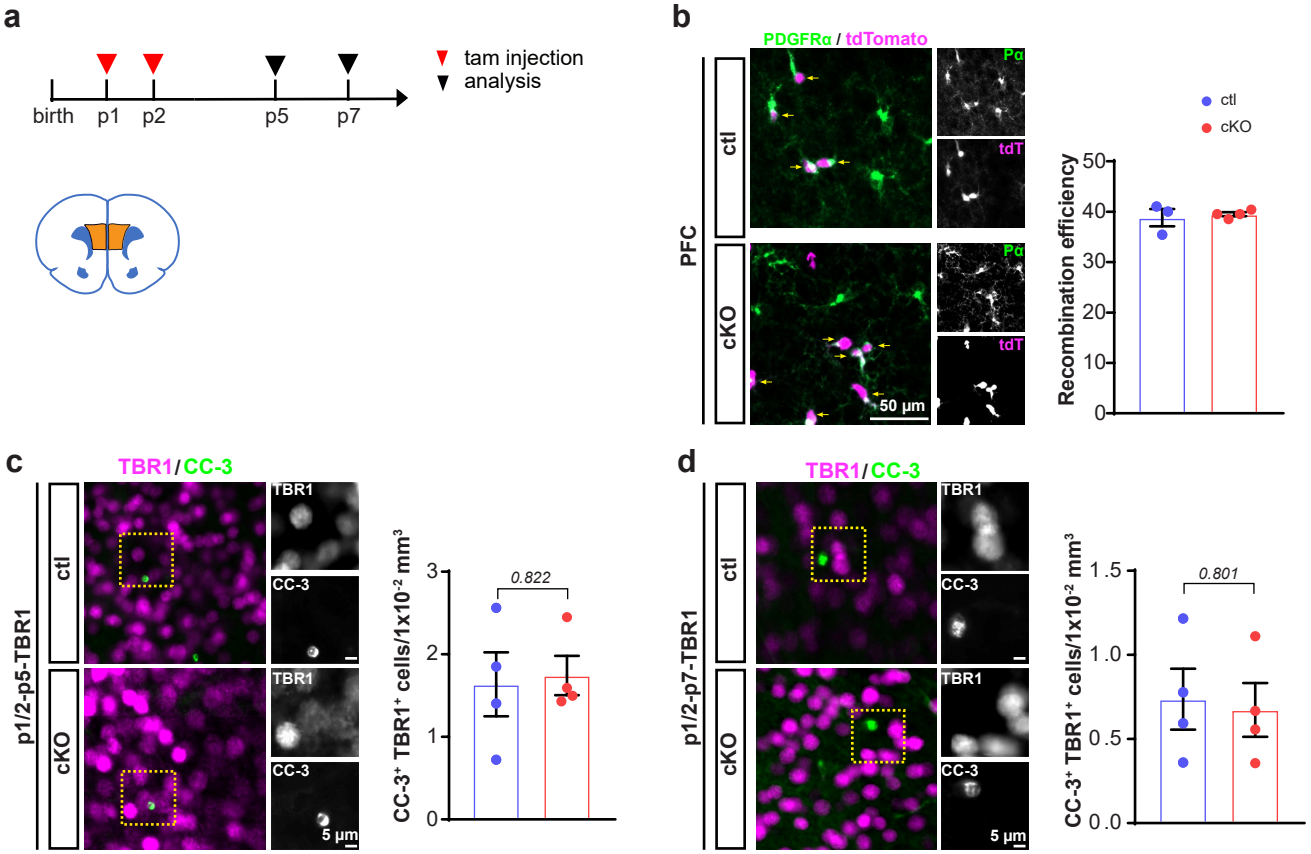

Supplementary figure 10

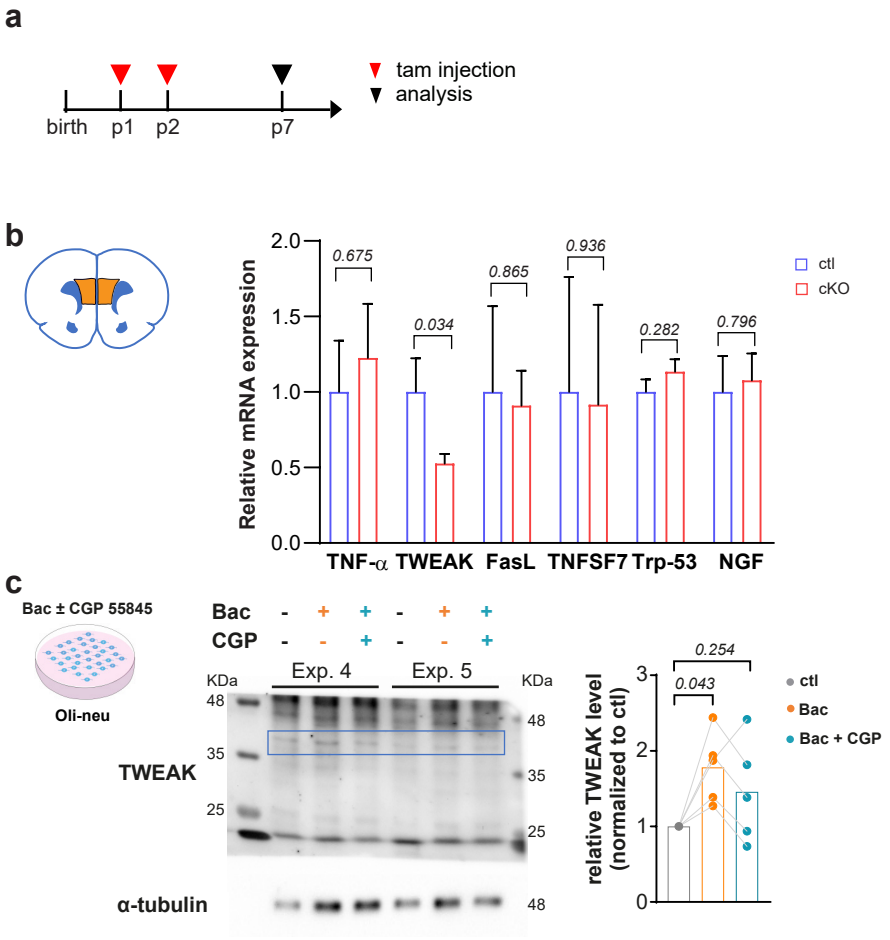

Supplementary figure 11

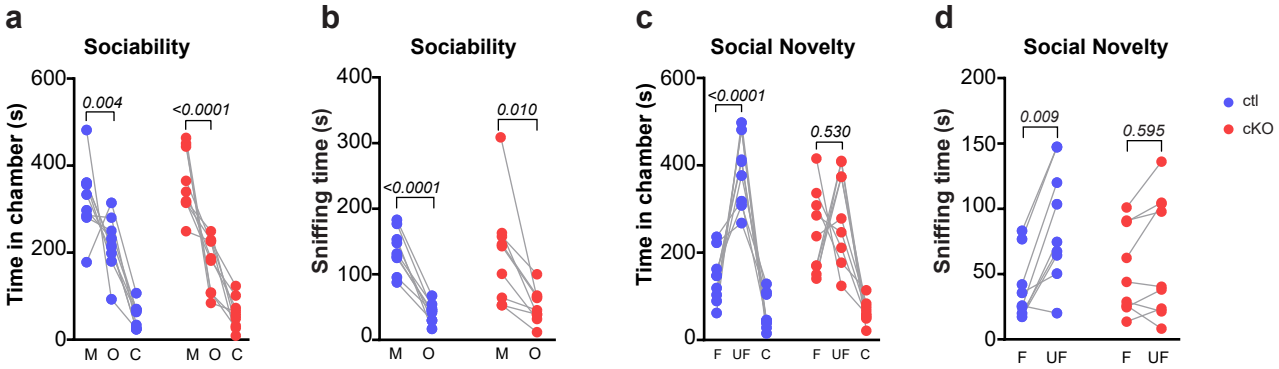

Supplementary information for

Impaired bidirectional communication between interneurons and oligodendrocyte precursor cells affects cognitive behavior

Lipao Fang[1], Na Zhao[1], Laura C. Caudal[1], Renping Zhao[2], Ching-Hsin Lin[3], Hsin-Fang Chang[3], Nadine Hainz[4], Carola Meier[4], Bernhard Bettler[5], Wenhui Huang[1], Anja Scheller[1], Frank Kirchhoff[1,*], Xianshu Bai[1,*]

1. Molecular Physiology, CIPMM, University of Saarland, 66421 Homburg, Germany
2. Biophysics, CIPMM, University of Saarland, 66421 Homburg, Germany
3. Cellular Physiology, CIPMM, University of Saarland, 66421 Homburg, Germany
4. Department of Anatomy and Cell Biology, University of Saarland, 66421 Homburg, Germany
5. Department of Biomedicine, University of Basel, 4056 Basel, Switzerland

Correspondence to:

Prof. Dr. Frank Kirchhoff,
Molecular Physiology,
CIPMM, University of Saarland,
66421 Homburg, Germany
frank.kirchhoff@uks.eu

Dr. Xianshu Bai
Molecular Physiology,
CIPMM, University of Saarland,
66421 Homburg, Germany
xianshu.bai@uks.eu

Materials and Methods

Ethics statement

Animal husbandry and procedures were performed at the animal facility of CIPMM, University of Saarland according to European and German guidelines for the welfare of experimental animals. Animal experiments were approved by the Saarland state's ''Landesamt für Gesundheit und Verbraucherschutz" in Saarbrücken/Germany (animal license number: 65/2013, 12/2014, 34/2016, 36/2016 and 08/2021).

Animals

To conditionally knock out (cKO) $GABA_{B1}$ receptors in oligodendrocyte precursor cells (OPCs), TgH(NG2-Cre^{ERT2})[1] mice were crossbred to $GABA_{B1}{}^{lox511/lox511}$ mice (flanking exon 7 and 8 of *gabbr1*)[2]. Mice with genotypes of $NG2^{ct2/wt}$ x $GABA_{B1}R^{fl/fl}$ were used as cKO and the littermates $NG2^{wt/wt}$ x $GABA_{B1}R^{fl/fl}$ or $NG2^{ct2/wt}$ x $GABA_{B1}R^{wt/wt}$ were controls after tamoxifen application. To visualize the recombined cells, we crossbred the double transgenic mice with TgH(Rosa26-CAG-$^{fl}STOP^{fl}$-tdTomato) (Rosa26-tdTomato) [3].

For oligodendrocyte specific deletion of $GABA_{B1}R$, we took advantage of TgN mice (PLP-Cre^{ERT2}) [4] crossbred with $GABA_{B1}{}^{lox511/lox511}$. Similarly, $PLP^{ct2/wt}$ x $GABA_{B1}R^{fl/fl}$ mice were used as cKO, while $PLP^{wt/wt}$ x $GABA_{B1}R^{fl/fl}$ or $PLP^{ct2/wt}$ x $GABA_{B1}R^{wt/wt}$ were controls after tamoxifen application.

Mouse ages are indicated in the main text and figure legends. Behavioral tests were carried out only with male mice at the age of 9 weeks, while both genders were used in the other experiments.

Tamoxifen administration

Tamoxifen was dissolved in Miglyol (3274, Caesar & Loretz GmbH) to a final concentration of 10 mg/ml. Tamoxifen was intraperitoneally injected to the mice depending on the body weight (100 mg/kg body weight). The time points of injections are indicated in the figures. Only for the pups treated at postnatal day 1 (p1) and 2, tamoxifen was injected to the lactating mother with

53 the same protocol [5]. For 4-week-old mice, tamoxifen was injected once per day for five
54 consecutive days [6].

55 **Immunohistochemistry**

56 Mice were perfused with PBS and 4 % paraformaldehyde (PFA). Mouse brains were post fixed
57 with 4 % PFA at 4°C overnight. Free floating brain slices (40 μm thickness) were cut in coronal or
58 sagittal sections using a Leica VT1000S vibratome. For immunocytochemistry, cells on coverslips
59 were fixed with ice cold 4 % PFA for 15 min. Slices or coverslips were incubated with blocking
60 solution containing 5 % horse serum and 0.5 % Triton X-100 at room temperature (RT) for 1 hour
61 (hr), followed by primary antibody incubation at 4 °C overnight and secondary antibody incubation
62 at RT for 2 hrs in blocking solution. Primary and secondary antibodies are listed in the
63 **Supplementary table 1 and 2,** respectively**.**

64 **Magnetic cell separation (MACS) of OPCs**

65 MACS sorting of OPCs was performed according to the manufacturer's instruction (Miltenyi
66 Biotec) with some modifications. Mice were perfused with cold Hank's balanced salt solution
67 without calcium and magnesium (HBSS, H6648, Gibco) and cortices were dissected in ice cold
68 HBSS. After the removal of debris (130-107-677, Miltenyi Biotec), cells were resuspended with
69 1 mL "re-expression medium" containing NeuroBrew-21 (1:50 in MACS neuro Medium) (130-093-
70 566 and 130-093-570, Milteny Biotec) and 200 mM L-glutamine (1:100, G7513, Sigma) at 37 °C
71 for 30 min. Cells were then incubated with Fc-receptor blocker for 10 min at 4 °C (provided with
72 CD140 microbeads kit), followed by a 15 min incubation with 10 μL microbeads mixture
73 composed of CD140 (130-101-502), NG2 (130-097-170) and O4 (130-096-670) in 1:1:1 at 4 °C.
74 For the purity assessment, cells were re-suspended with 1 mL "re-expression medium," seeded
75 on the coverslips which were coated with polyonithin (P2533, Sigma). After 2 hrs incubation at
76 37 °C with 5 % CO_2, cells were processed for immunocytochemistry against PDGFRα and DAPI.
77 For qRT-PCR or Western blot analysis, MACS sorted OPCs were lysed by RIPA buffer (89900,
78 Thermo Scientific).

79 **Western blot analysis**

80 Deeply anesthetized mice were perfused with cold PBS. Medial prefrontal cortices (mPFC) and
81 corpus callosa (cc) were dissected in ice cold PBS. Tissues were homogenized with sucrose lysis
82 buffer (320 mM sucrose, 10 mM Tris-HCl, 1 mM $NaHCO_3$ (pH=7.4); 1 mM $MgCl_2$), and MACS-
83 sorted OPCs were lysed with RIPA buffer. Both buffers were supplemented with 1 X protease
84 inhibitors (05892970001 Roche) and 1 X phosphatase inhibitor (04906837001, Roche). Protein
85 (5 µg) was blotted onto nitrocellulose transfer membranes (QP0907015, qpore). Membrane was
86 blocked with 5 % non-fat milk or 5 % BSA (A7906, Sigma) diluted in 0.1 % TBST. Primary
87 antibodies were diluted with corresponding blocking buffer. Primary antibodies used for Western
88 blot are listed in the **Supplementary table 3.**

89 Secondary antibodies were: HRP anti-mouse (1:2000,) and anti-rabbit (1:2000). Membranes were
90 illuminated with WesternBright Chemilumineszenz Substrat Quantum kit (541015, Biozym) and
91 documented with ChemiDoc-MP.

92 **Quantitative real time PCR**

93 Brain tissue or the MACS-sorted OPCs were homogenized as described above. NucleoSpin RNA
94 Plus XS kit (740990.50, Macherey-Nagel) was used to extract mRNA and Omniscript kit (205113,
95 QIAGEN) was used for reverse transcription. RT-PCR was performed using EvaGreen (27490,
96 Axon) kit. Primer sequences for qRT-PCR are listed in **Supplementary table 4**.

97 **Electrophysiology**

98 **Slice preparation:** Mice were anesthetized by isoflurane before decapitation, and brain was
99 quickly isolated and immersed in an ice-cold, oxygenated (5 % CO_2/95 % O_2, pH=7.4) solution
100 containing (in mM) 87 NaCl, 3 KCl, 25 $NaHCO_3$, 1.25 NaH_2PO_4, 3 $MgCl_2$, 0.5 $CaCl_2$, 75 sucrose
101 and 25 glucose. Coronal or semi-sagittal slices in 300 µm thickness were prepared with vibratome
102 (Leica VT 1200S, Nussloch, Germany) and transferred to a nylon basket slice holder for
103 incubation in artificial cerebral spinal fluid (ACSF) containing (in mM) 126 NaCl, 3 KCl,

104 25 $NaHCO_3$, 15 glucose, 1.2 NaH_2PO_4, 2 $CaCl_2$, and 2 $MgCl_2$ at 32 °C for 0.5 h. Subsequently,
105 slices were removed from the water bath and kept at RT with continuous oxygenation prior to use.

106 **IPSCs and EPSCs recordings:** Semi-sagittal slices were transferred to the recording chamber
107 that was continuously perfused with oxygenated ACSF containing 1 $MgCl_2$ and 2.5 $CaCl_2$ at a
108 flow rate of 2-5 mL/min. During recordings, 50 μM strychnine and 50 μM picrotoxin were added
109 to block inhibitory synaptic transmission. Pyramidal neurons were identified morphologically
110 (Axioskop 2 FS mot, Zeiss, Jena, Germany) with a 40x water immersion objective. Tissue was
111 detected with a QuantEM 512SC camera (Photometrics, Tucson, USA). Whole-cell membrane
112 currents were recorded by an EPC 10 USB amplifier (HEKA, Lambrecht, Germany), low pass
113 filtered at 3 kHz and data acquisition was controlled by Patchmaster software (HEKA). The
114 resistance of patch pipettes (7–9 ΩM) were fabricated from borosilicate capillaries (OD: 1.5 mm;
115 Sutter, USA) using a Micropipette Puller (Model P-97, Sutter Instrument Co., CA). Patch pipettes
116 were filled with the solution containing (in mM) 125 cesium gluconate, 20 tetraethylammonium
117 (TEA), 2 $MgCl_2$, 0.5 $CaCl_2$, 1 EGTA, 10 HEPES and 5 Na_2ATP (pH=7.2). Spontaneous excitatory
118 and inhibitory postsynaptic currents (sEPSCs, sIPSCs) of pyramidal neurons in mPFC were
119 recorded for 40 s in voltage-gated mode at a holding potential of -70 mV and +30 mV,
120 respectively. Currents above 10pA were analyzed with MATLAB. EPSCs of pyramidal neurons in
121 the layer V of mPFC were recorded by stimulating presynaptic axons in the layer II/III of mPFC
122 with a concentric bipolar microelectrode (MicroProbes, USA). Stimulus duration was 200 μs. To
123 estimate short-term plasticity, 40 trains of stimulation were applied to induce synaptic depression,
124 and the depressing trains were repeated with frequency of 10 Hz and an interval of 20 s to allow
125 for recovery from synaptic depression. The stimulation threshold was applied from 30 μA to
126 80 μA. IPSCs were conducted in the same region, however with a holding potential of 0 mV.

127 **Compound action potential recordings:** Compound action potentials were recorded in the
128 corpus callosum as previously described (Crawford et al., 2009). Micropipettes with 1-3 MΩ

129 resistance were filled with ACSF. Inward responses were evoked in current-clamp mode by
130 varying the intensity of stimulus pulses (0.2-4.0 mA) at 1 mm distance between recording and
131 stimulation electrodes, with a stimulus duration of 200 µs. The sample sweeps were acquired
132 every 5 s. Conduction velocity was estimated by changing the distance from 2.5 mm to 0.5 mm
133 between the stimulating and recording electrodes with a constant stimulus. To enhance the signal
134 to noise ratio, we averaged at least 15 successive sweeps. Data analysis was performed with
135 Igor pro 6.3.7.2 (WaveMetrics, Oregen, US).
136 All the experiments were conducted at RT (22 – 24 °C).
137 **Data analysis:** Data generated by Patch Master were loaded into MATLAB (Mathworks, MA,
138 USA) with a module adapted from sigTOOL (Lidierth, 2009). Evoked EPSC and IPSC traces from
139 the same cells were manually checked and pooled. The average of EPSC/IPSC traces from each
140 cell was used for analysis. Data analysis was performed using routines that were custom written
141 in Matlab.
142 **EEG telemetry and analysis**
143 Telemetric EEG transmitter implantation was adapted from Bedner and colleagues [7]. Mice were
144 implanted with telemetric EEG transmitters (DSI PhysioTel® ETA-F10, Harvard Biosciences, Inc.
145 Holliston, Massachusetts, USA) between 8 and 10 weeks of age. The animals were placed in a
146 stereotaxic frame (Robot stereotaxic, Neurostar, Tübingen, Germany) for implantation of depth
147 electrodes at 3.4 mm posterior to bregma and bilaterally 1.6 mm from the sagittal suture. After
148 post-surgical care and recovery, cages were placed on individual radio receiving plates (DSI
149 PhysioTel® RPC-1, Data Sciences International, St. Paul, USA) for synchronized EEG and video
150 recording (MediaRecorder Software, Noldus Information Technology, Wageningen, Netherlands).
151 EEG and video recording were performed for 24 hrs.
152 **Data analysis:** EEG traces were analysed with the Neuroscore software (Version 3.3.1., Data
153 Sciences International, St. Paul, USA). After applying a general Notch filter (50 Hz band stop),
154 relative power band values were determined with order 13 fast-Fourier transform in 10s epochs

155 and later averaged per hour of recording. Statistical analysis was performed with GraphPad
156 Prism.

157 **Behavioral analysis**

158 Several behavioral tests were performed with the same cohorts of mice (male, 9-week-old). The
159 order of the tests was designed from low to high invasiveness to reduce the interference from the
160 prior tests. The chamber or tested square was wiped with 75 % ethanol before tests to remove
161 odors.

162 **Nest building test:** The nest building test was carried out as previously described [8]. Mice were
163 moved into new single cages in the behavior testing room for habituation. After 24 h, a piece of
164 pressed cotton in size of 7x5 cm2 was placed in the cage. After 14 h, the shape and weight of the
165 cotton was recorded and unbiasedly scored according to the criteria [8].

166 **Open field test:** The mice were put in the open field maze, which measured 50 cm (length) x 50
167 cm (width) x 38 cm (height). Mice could move and explore freely for 10 min in the open field
168 square. In each test, the single mouse was put in the center of the square arena. The videos of
169 these 10 min were recorded (USB webcam) and analyzed (EthoVision XT 11.5, Noldus
170 Technology). Duration time in the center area (s), moved distance (cm) and speed (cm/s) were
171 determined [9]

172 **New object recognition test:** The mice could freely explore the two identical objects placed at a
173 distance of 8.5 cm from the side walls in two opposite corners of the apparatus for 10 min. After
174 40 min, one of the objects was replaced by a novel one, and the test mouse was allowed to
175 explore again. Preference index was defined as the percentage of the time exploring one identical
176 object within the total time exploring both objects. Recognition index was defined as the
177 percentage of the time exploring the novel object among the total time of exploring both objects.

178 **Three chamber social behavior test:** The three-chamber box was employed for social
179 behavioral studies [10]. Three chambers were equally sized and separated by two walls evenly
180 distributed in the box. A square door at the bottom center of each door allowed free running of

181 the mice within the three chambers. Two empty wire cages were placed at the side chambers,
182 leaving the center chamber empty. For habituation, mice were kept in the center chamber for
183 10 min, followed by a 10 min-habituation session with access to all three chambers. For the
184 sociability test, the test mouse was placed in the center chamber, while a mouse of similar age
185 was kept under the stainless wire cage in one of the side chambers. The other chamber contained
186 an empty wire cage. For 10 min, the test mouse could select freely all three chambers. For the
187 social novelty test, a novel mouse was placed under the other empty cage being an unfamiliar
188 mouse, and the prior mouse as familiar one. The test mouse was again allowed to freely explore
189 both animals for 10 min. The experiment was recorded with video camera and the time that the
190 test mouse spent in each chamber and the time of sniffing was analyzed.

191 **Cell culture**

192 **Cell line Oli-neu:** The murine oligodendroglial precursor cell line Oli-neu [11] was kindly provided
193 by Professor Jacqueline Trotter (University of Mainz). Undifferentiated Oli-neu cells were
194 incubated at 37 °C and 5 % CO_2 in poly-L-lysine (Merck) coated cell culture flasks (Greiner Bio
195 one) for expansion or cell culture dishes (Greiner Bio one) for experiments. Sato medium
196 consisting of DMEM high glucose medium (Fisher Scientific) with supplementation of 10 µg/ml
197 transferrin (Sigma), 10 µg/ml insulin (Santa Cruz), 100 µM putrescine (Sigma), 200 nM
198 progesterone (Sigma), 500 nM tri-iodo-thyrodine (Sigma), 220 nM sodium selenite (Sigma),
199 520 nM L-thyroxine (Sigma) and 1.5 % normal horse serum (Fisher Scientific) was used for
200 culturing and proliferation of cells. For experiments, $2x10^5$ cells were seeded in a 60 mm Petri
201 dish. 48 hours later, the medium was changed to fresh, with or without CGP 55845 (50 µM) for
202 24 hours. Cells were lysed with Qiazol (Qiagen) for qRT-PCR in a blind manner. Conditional
203 medium of control cells was collected for further neuronal treatment.

204 **Primary culture of cortical neurons:** Cortical neurons were isolated from p0 pups (C57BL/6
205 mouse strain). Briefly, the cortex was dissected from the whole brain in ice cold Earle's Balanced
206 Salt Solution (EBSS, Gibco). The cortex was then digested with 35 units papain (Worthington,

207 NJ) for 45 min at 37 °C, followed by gentle mechanical trituration. 1x105 cells were seeded on
208 25 mm glass coverslips in 24-well culture plates for further immunostaining. The glass coverslips
209 were pre-coated with a mixture of coating solution containing 17 mM acetic acid, poly-D-Lysine
210 (Sigma, P6407) and collagen I (Gibco, A1048301). Neurons were cultured in NBA culture medium
211 that contained 10 % FCS, 1 % penicillin-streptomycin, 1 % GlutaMAX and 2 % B-27 supplement
212 (Gibco) for 7 d at 37 °C with 5 % CO_2 incubator before the experiment. To examine the effect of
213 TWEAK on neurons, conditioned Oli-neu culture medium supernatant or Sato, was applied to
214 neuron NBA culture medium, with a ratio of 1:2 to NBA resulting in 1 ml medium per 24-well and
215 2 ml medium per 6-well. Cells were collected after 6 h with different culture condition with or
216 without 20 μM TWEAKR inhibitor L524-0366 (509374, Calbiochem) for further analysis.

217 **Image acquisition and analysis**

218 Brain slices were scanned with the fully automated slide scanner AxioScan.Z1 (Zeiss, Jena) and
219 LSM 710 confocal microscope (Zeiss, Jena). Cell counting was manually performed without bias
220 by using ZEN software (Zeiss, Jena). The lengths of nodes and paranodes were measured using
221 the 'straight' tool of Fiji software. The Imaris (version 9.6) with functions of volume analysis and
222 vesicle classification were used for MBP-PV (Fig. 1M, N) and vGAT study (Fig. F-I). Cell counting
223 and Imaris analysis were carried out in a blind manner.

224 **Bromodeoxyuridine assay**

225 Adult animals received 1 mg/ml bromodeoxyuridine (BrdU) (B5002, Sigma-Aldrich, St. Louis, MO)
226 dissolved in drinking water for seven consecutive days. For juvenile mice, single shot of 10 mg/ml
227 BrdU dissolved in 0.9 % NaCl were intraperitoneally injected to the p13 pups and analyzed at
228 p14.

229 **Electron microscopy**

230 **Perfusion & dissection:** Anesthetized (Ketamine/Xylazine in 0.9% NaCl solution (all: Bayer,
231 Leverkusen, Germany)) mice were intracardially perfused with buffered heparin (B. Braun,
232 Melsungen, Germany) solution (end concentration 50 IU/mL) followed by perfusion fixation with

233 4% (w/v) paraformaldehyde and 0.5% (w/v) glutaraldehyde in 0.1M cacodylate buffer. During
234 perfusion, the solutions were gradually cooled down from 37°C to ice cold temperatures. Whole
235 brains were dissected, immersed in fixative solution for 24h, and stored in 0.1M cacodylate buffer
236 at 4°C until further use.

237 **Slicing:** For vibratome slicing, whole brains were embedded in 10% gelatin and immersed in ice
238 cold 0.1M cacodylate buffer. 500 µm frontal sections were made using a vibratome (VT1000S,
239 Leica Microsystems, Wetzlar, Germany) at a frequency of 80Hz and 0.1mm/s speed. Slices
240 containing the region of interest were determined using a mouse brain atlas [12], and particular
241 brain areas (i.a. corpus callosum) were meticulously cut out using a fine scalpel.

242 **Embedding & examination:** The specimen of the different brain regions were embedded for
243 electron microscopy (1975) [13]. In short, samples were repeatedly rinsed in 0.1M cacodylate buffer,
244 osmicated in 2% osmium tetroxide in 0.1M cacodylate buffer for 1h, washed in distilled water, and
245 dehydrated in an ascending series of ethanol (70% to 100%) and acetone (100%, water-free). An
246 embedding in Epon resin (EMS, Hatfield, PA, USA) followed. After thorough polymerization, semi-
247 thin (300nm) and ultra-thin (65nm) sections were cut using an ultra-microtome (EM UC7, Leica
248 Microsystems, Wetzlar, Germany). Semi-thin sections were stained with Richardson blue staining
249 solution, and examined under a light microscope (DM2500, Leica Microsystems, Wetzlar,
250 Germany). Ultra-thin sections were contrasted with 5% lead citrate for 5min, examined with a
251 transmission electron microscope (Tecnai G2, FEI, Hillsboro, OR, USA), and randomly selected
252 areas were documented with a digital camera (MegaView III, Olympus, Shinjuku, Japan).

253 **Statistics**

254 Prior to statistical analysis, data were tested for outlier identification and Gaussian distribution
255 with GraphPad Prism 8. Statistical differences were indicated in the figures and legends. Each
256 data point in the graphs indicates biological individuals. Exceptions are indicated in the figure
257 legends.Data are shown as mean±SEM, except for violin plots (Fig. 2i and Fig. 4b). The median
258 and quartiles are indicated as thick and thin dashed lines, respectively.

References

1. Huang, W., *et al.* Novel NG2-CreERT2 knock-in mice demonstrate heterogeneous differentiation potential of NG2 glia during development. *Glia* **62**, 896-913 (2014).
2. Haller, C., *et al.* Floxed allele for conditional inactivation of the GABAB(1) gene. *Genesis* **40**, 125-130 (2004).
3. Madisen, L., *et al.* A robust and high-throughput Cre reporting and characterization system for the whole mouse brain. *Nat Neurosci* **13**, 133-140 (2010).
4. Leone, D.P., *et al.* Tamoxifen-inducible glia-specific Cre mice for somatic mutagenesis in oligodendrocytes and Schwann cells. *Mol Cell Neurosci* **22**, 430-440 (2003).
5. Huang, W., *et al.* During Development NG2 Glial Cells of the Spinal Cord are Restricted to the Oligodendrocyte Lineage, but Generate Astrocytes upon Acute Injury. *Neuroscience* **385**, 154-165 (2018).
6. Jahn, H.M., *et al.* Refined protocols of tamoxifen injection for inducible DNA recombination in mouse astroglia. *Sci Rep* **8**, 5913 (2018).
7. Bedner, P., *et al.* Astrocyte uncoupling as a cause of human temporal lobe epilepsy. *Brain* **138**, 1208-1222 (2015).
8. Deacon, R.M. Assessing nest building in mice. *Nat Protoc* **1**, 1117-1119 (2006).
9. Seibenhener, M.L. & Wooten, M.C. Use of the Open Field Maze to measure locomotor and anxiety-like behavior in mice. *J Vis Exp*, e52434 (2015).
10. Kaidanovich-Beilin, O., Lipina, T., Vukobradovic, I., Roder, J. & Woodgett, J.R. Assessment of social interaction behaviors. *J Vis Exp* (2011).
11. Jung, M., *et al.* Lines of murine oligodendroglial precursor cells immortalized by an activated neu tyrosine kinase show distinct degrees of interaction with axons in vitro and in vivo. *Eur J Neurosci* **7**, 1245-1265 (1995).
12. Franklin, K. & Paxinos, G. *The mouse brain in stereotaxic coordinate* (Academic press, 2007).
13. Glauert, A.M. *Fixation, Dehydration and Embedding of Biological Specimens. Practical methods in electron microscopy.* (North-Holland Publishing Company, 1975).

292 **Supplementary table 1: Primary antibodies used for immunostaining**

Antibodies	Host	Dilutions	Cat.No.	Company	PRID
PDGFRα	goat	1:500	AF1062	R&D Systems	AB_2236897
adenomatous polyposis coli clone 1(CC1)	mouse	1:200	OP80	Calbiochem	AB_2057371
Olig2	rabbit	1:500	AB9610	Millipore	AB_570666
MBP	mouse	1:500	SMI99	Biolegend	AB_10120130
Parvalbumin	rabbit	1:1000	PV 25	Swant	AB_10000344
Parvalbumin	mouse	1:500	P3088	Sigma	AB_477329
Caspr	rabbit	1:500	ab34151	abcam	AB_869934
DsRed	rabbit	1:1000	632496	Clontec	AB_10013483
BrdU	rat	1:1000	ab6326	abcam	AB_305426
Cleaved Caspase-3	rabbit	1:200	9661	Cell Signaling Technology	AB_2341188
Cleaved Caspase-3	mouse	1:100	STJ9744	St. John's Laboratory	
GAD67	mouse	1:500	MAB5406	Millipore	AB_2278725
NeuN	mouse	1:500	MAB377	Millipore	AB_2298772
CTIP2	rat	1:200	650601	Biolegend	AB_10896795
TBR1	rabbit	1:500,	49661	Cell Signaling Technology	AB_2799364
vGAT	mouse	1:500	13002	Synaptic Systems	AB_887871
FN14	mouse	1:50	314108	Biolegend	AB_2810477

293

294 **Supplementary table 2: Secondary antibodies used for immunostaining**

Antibodies	Fluorophore	Cat. No.	Company
Donkey anti-mouse	Alexa Fluor® 488		Thermofischer
	Alexa Fluor® 546	A10036	
	Alexa Fluor® 647	A31571	
	DyLight® 755	SA5-10171	Invitrogen
Donkey anti-rabbit	Alexa Fluor® 488	A21206	Thermofischer
	Alexa Fluor® 546	A10040	
	Alexa Fluor® 647	A31573	
	Alexa Fluor® 790	A11374	
Donkey anti-goat	Alexa Fluor® 488	A11055	Thermofischer
	Alexa Fluor® 546	A11056	
	Alexa Fluor® 647	A21447	
	Alexa Fluor® 750	ab175744	abcam
Donkey anti-rat	DyLight-755	SA5-10031	Thermofischer
DAPI (25ng/ml**)**		A10010010	biochmica

295

296 Secondary antibodies were diluted 1:1000 with the blocking buffer.

297

298 **Supplementary Table 3. Primary antibodies used for Western blot**

Antibodies	Host	Dilutions	Cat.No.	Company	PRID
$GABA_{B1}R$	mouse	1:500	ab55051	abcam	AB_941703
GAPDH	mouse	1:2000	G8795	Sigma	AB_1078991
MBP	mouse	1:1000	SMI99	Biolegend	AB_10120130
Tubulin-α	rabbit	1:2000	T6074	Sigma	AB_477582
TWEAK	rabbit	1:500	NBP1-76695	Novus Biologicals	AB_11036308

299

300

301 **Supplementary Table 4. Primers used for qRT-PCR**

Gene	Forward	Reverse
$GABA_{B1}$ R	5'-CGAAGCATTTCCAACATGAC-3'	5'-CAAGGCCCAGATAGCATCATA-3'
β-actin	5'-CTTCCTCCCTGGAGAAGAGC-3'	5'-ATGCCACAGGATTCCATACC-3'
TNF-α	5'-GACGTGGAACTGGCAGAAGAG-3'	5'-TTGGTGGTTTGTGAGTGTGAG-3'
TWEAK	5'-CCGCCAGATTGGGGAATTTAC-3'	5'-AGTCCAAAGTAGGTTAGGAAGGG-3'
FasL	5'-TCCGTGAGTTCACCAACCAAA-3'	5'-GGGGGTTCCCTGTTAAATGGG-3'
TNFSF7	5'-TGTAGCGGACTACTCAGTAAGC-3'	5'-TGGGGTCCTTCCGAGGAAC-3'
Trp53	5'-CTCTCCCCCGCAAAAGAAAAA-3'	5'-CGGAACATCTCGAAGCGTTTA-3'
NGF	5'-TGATCGGCGTACAGGCAGA-3'	5'-GCTGAAGTTTAGTCCAGTGGG-3'

302